nant negative RinS34N potently inhibits NGF-induced neurite outgrowth. This may be due to the fact that RinS34N has some toxic effect to the cells. Moreover, we (this paper) and Spencer et al. (2002) observed that neither wild-type nor constitutively active Rin induced MAPK activation. It has been shown that sustained MAPK activation is necessary for NGF-stimulated neurite outgrowth (Marshall, 1995). Thus, we consider that Rin is not likely to be a component of the NGF–MAPK pathway leading to neurite outgrowth.

We have demonstrated that dominant negative RinG29V-C-7 or siRNA of Rin inhibits the forskolin plus KCl-induced neurite outgrowth at the level of stimulation of forskolin alone, and that Rin exists in a calcium-mediated signaling pathway using calcium channel blockers. The importance of this calcium–cAMP signaling pathway is illustrated by Wong's report. Wong et al. (1999) showed that calcium-stimulated adenylate cyclase activity is essential for long-term memory and late phase long-term potentiation. Intracellular calcium increase through voltage-dependent calcium channels or *N*-methyl-D-aspartate receptors can activate calcium-sensitive adenylate cyclase, and generated cAMP can activate protein kinase A or cyclic AMP response element binding protein–mediated transcription pathway leading to long-term potentiation and memory formation (Wong et al., 1999; Poser and Storm, 2001). Thus, Rin may play a role in a long term effect on neuronal function as well as neuritogenesis.

In conclusion, we have identified a novel function of Rin protein, i.e., inducing neurite outgrowth in PC12 cells. However, many problems about Rin signaling, for example, whether there is a specific GEF or GAP of Rin, remains to be clarified. Further studies focusing on these problems will shed light on our understanding of the Rin-signaling pathway and its roles in the regulation of neuronal cell morphology and the functions of the nervous system.

Materials and methods

Antibodies and reagents

Anti–c-Myc 9E10 antibody, anti-Cdc42 antibody and anti-RhoA antibody were purchased from Santa Cruz Biotechnology, Inc. Anti-HA high affinity antibody (3F10) was purchased from Roche. Antineurofilament 160 antibody (NN18), NGF, ionomycin, LPA, W12 (*N*-[4-aminobutyl]-2-naphthalenesulfonamide), W13 (*N*-[4-aminobutyl]-5-chloro-2-naphthalenesulfonamide), nitrendipine, diltiazem, and CaM-conjugated agarose were purchased from Sigma-Aldrich. Anti-Rin antibody and MAPK kinase inhibitor U0126 were purchased from Calbiochem. Antiphospho-p44/42 MAPK antibody was purchased from Cell Signaling Technology. Anti-MAPK 1/2 and anti-Rac 23A8 antibodies were purchased from Upstate Biotechnology. Cy3-conjugated secondary antibody was purchased from CHEMICON International, Inc. FITC-conjugated secondary antibody was purchased from Zymed Laboratories. pGFP-C1 vector was purchased from CLONTECH Laboratories, Inc. pGEX vector and glutathione-Sepharose beads were purchased from Amersham Biosciences.

Expression plasmids

Myc-Rin and HA-Rin mammalian expression pEF-Bos vectors were constructed as described previously (Hoshino and Nakamura, 2002). The dominant negative Rac1 vector (pEF-Bos Myc-RacS17N) and Cdc42 vector (pEF-Bos Myc-Cdc42S17N) were provided by Y. Takai (Osaka University, Osaka, Japan) and H. Miki (University of Tokyo, Tokyo, Japan). Constitutively active Rin mutants (RinQ78L and RinG29V), Rin deletion mutant (RinΔ18), Rin point mutants (RinC-7 and RinC-4), and dominant negative Rin mutants (RinS34N and RinG29V-C-7) were generated by PCR-based site-directed mutagenesis. The dominant negative PAK1 vector was constructed as described previously (Zhao et al., 1998). The coding region of all constructs was confirmed by DNA sequencing.

Cell cultivation and transfection

Cos-7 cells and PC12 cells were cultured in DME (Nissui) supplemented with 10% FBS (Intergen), 2 mM L-glutamine and penicillin/streptomycin, and incubated at 37°C in an atmosphere of 5% CO_2. Serum-starved cells were obtained by incubation for 24 h in the medium containing 0.5% serum. Semi-confluent cells were transiently transfected with expression vectors using Lipofectamine 2000 (Invitrogen) according to the manufacturer's instructions.

CaM-binding assay

The CaM-binding assay was performed as described previously (Hoshino and Nakamura, 2002).

Measurement of endogenous Rac/Cdc42 activity

The CRIB domain of PAK1 was cloned into the pGEX vector and was expressed in *Escherichia coli* as a fusion protein. Transfected PC12 cells were serum starved for 24 h and lysed with an ice-cold lysis buffer (50 mM Tris-HCl, pH 7.5, 500 mM NaCl, 2.5 mM $MgCl_2$, 10% glycerol, 1% NP-40, 10 mM NaF, 1 mM Na_3VO_4, 0.1 mM PMSF, and 10 μg/ml aprotinin and leupeptin). Cell lysates were centrifuged for 10 min at 13,000 *g* at 4°C, and each supernatant was incubated with 10 μg of purified GST-PAK CRIB immobilized on glutathione-Sepharose beads at 4°C for 30 min. After the beads were washed twice with a lysis buffer, the bound proteins were suspended in 20 μl Laemmli sample buffer and separated by 14% SDS-PAGE.

Measurement of endogenous Rho activity

Rho pull-down assay was performed similar to the Rac/Cdc42 pull-down assay as described in the previous paragraph, using Rho-binding domain of GST-mDia1 protein instead of GST-PAK CRIB protein. The beads-bound Rho proteins were visualized by Western blotting using anti-RhoA antibody.

Western blotting

Protein samples were separated by SDS-PAGE, transferred to nitrocellulose membrane (Schleicher and Schuell), and probed with a primary antibody in PBS containing 0.1% Tween 20 and 5% nonfat dry milk (Becton Dickinson). The primary antibody was visualized with HRP-conjugated secondary antibody (Amersham Biosciences) and ECL (PerkinElmer).

RT-PCR

Total RNA was extracted from the cells using Isogen reagent (Wako). 5 μg of extracted total RNA was used as a template for oligo-dT–primed first-strand cDNA synthesis using SuperScript reverse transcriptase (Invitrogen), and 2% of the resultant cDNA was used for PCR amplification. PCR was performed by 30 cycles at 94°C for 1 min, 55°C for 1 min, and 72°C for 1 min. The primers used were as follows: for Rin, forward, 5′-CTCTTGCTCGAGACTACAAC-3′ and reverse, 5′-CCTTCCTGCGTATTTCTCTC-3′ (105 bp); and for GAPDH, forward, 5′-CCTGCACCACCAACTGCTTAGC-3′ and reverse, 5′-GCCAGTGAGCTTCCCGTTCAGC-3′ (230 bp). The identity of the amplified cDNAs was confirmed by DNA sequencing.

Immunofluorescence and neurite outgrowth analysis

48 h after transfection, PC12 cells were washed with PBS buffer and fixed with 3% PFA-PBS for 20 min. Next, cells were membrane permeabilized in 0.2% Triton X-100 PBS for 5 min. After the residual PFA and Triton X-100 were washed away with PBS buffer, cells were probed with a primary antibody in PBS for 2 h, followed by incubation with secondary antibody for 2 h. Stained cells were examined under appropriate illumination on a fluorescence microscope (Carl Zeiss MicroImaging, Inc.). About 200 cells were counted at each experiment. Cells were counted as positive for neurite outgrowth if one or more neurites exceeded one cell body diameter in length.

RNA interference

Single-stranded RNA was synthesized by standard protocols (Elbashir et al., 2001). Complementary single-stranded RNAs were annealed by heating them to 90°C and cooling to 37°C. Disruption of Rin protein function was performed by transfecting double-stranded RNAs into cells using Lipofectamine 2000 reagent.

We thank all members of our laboratory for their valuable suggestions and Drs. N. Suzuki, Y. Matsumoto, S. Ishii, H. Bito, and T. Shimizu for their comments and continuous encouragement. We are grateful to Drs. Y. Takai and H. Miki for providing a dominant negative Rac1 and Cdc42 vectors. We also thank Ms. H. Izumi and N. Fukumoto for their skillful technical assistance.

This research was supported by an Advanced Brain Research grant from the Ministry of Education, Science, Sports, Culture, and Technol-

ogy, and Health Sciences Research grants from the Organization of Pharmaceutical Safety and Research and Research on Advanced Medical Technology, nano-001.

Submitted: 13 August 2003
Accepted: 8 October 2003

References

Bashour, A.M., A.T. Fullerton, M.J. Hart, and G.S. Bloom. 1997. IQGAP1, a Rac- and Cdc42-binding protein, directly binds and cross-links microfilaments. *J. Cell Biol.* 137:1555–1566.

Benard, V., B.P. Bohl, and G.M. Bokoch. 1999. Characterization of Rac and Cdc42 activation in chemoattractant-stimulated human neutrophils using a novel assay for active GTPases. *J. Biol. Chem.* 274:13198–13204.

Bishop, A.L., and A. Hall. 2000. Rho GTPases and their effector proteins. *Biochem. J.* 348:241–255.

Bos, J.L. 1998. All in the family? New insights and questions regarding interconnectivity of Ras, Rap1 and Ral. *EMBO J.* 17:6776–6782.

Curtis, J., and S. Finkbeiner. 1999. Sending signals from the synapse to the nucleus: possible roles for CaMK, Ras/ERK, and SAPK pathways in the regulation of synaptic plasticity and neuronal growth. *J. Neurosci. Res.* 58:88–95.

Elbashir, S.M., J. Harborth, W. Lendeckel, A. Yalcin, K. Weber, and T. Tuschl. 2001. Duplexes of 21-nucleotide RNAs mediate RNA interference in cultured mammarian cells. *Nature.* 411:494–498.

Fukata, M., T. Watanabe, J. Noritake, M. Nakagawa, M. Yamaga, S. Kuroda, Y. Matsuura, A. Iwamatsu, F. Perez, and K. Kaibuchi. 2002. Rac1 and Cdc42 capture microtubules through IQGAP1 and CLIP170. *Cell.* 109:873–885.

Greene, L.A., and A.S. Tischler. 1976. Establishment of a noradrenergic clonal line of rat adrenal pheochromocytoma cells which respond to nerve growth factor. *Proc. Natl. Acad. Sci. USA.* 73:2424–2428.

Hart, M.J., M.G. Callow, B. Souza, and P. Polakis. 1996. IQGAP-1, a calmodulin-binding protein with a rasGAP-related domain, is a potential effector for Cdc42Hs. *EMBO J.* 15:2997–3005.

Hidaka, H., and T. Tanaka. 1983. Naphthalenesulfonamides as calmodulin antagonists. *Methods Enzymol.* 102:185–194.

Hoshino, M., and S. Nakamura. 2002. The Ras-like small GTP-binding protein Rin is activated by growth factor stimulation. *Biochem. Biophys. Res. Commun.* 295:651–656.

Kaplan, D.R., and R.M. Stephens. 1994. Neurotrophin signal transduction by the Trk receptor. *J. Neurobiol.* 25:1404–1417.

Kato, H., H. Yasui, Y. Yamagichi, J. Aoki, H. Fujita, K. Mori, and M. Negishi. 2000. Small GTPase RhoG is a key regulator for neurite outgrowth in PC12 cells. *Mol. Cell. Biol.* 20:7378–7387.

Kaziro, Y., H. Itoh, T. Kozasa, M. Nakafuku, and T. Satoh. 1991. Structure and function of signal-transducing GTP-binding proteins. *Annu. Rev. Biochem.* 60:349–400.

Kimura, K., T. Tsuji, Y. Takada, T. Miki, and S. Narumiya. 2000. Accumulation of GTP-bound RhoA during cytokinesis and a critical role of ECT2 in this accumulation. *J. Biol. Chem.* 275:17233–17236.

Kobayashi, M., S. Nagata, Y. Kita, N. Nakatsu, S. Ihara, K. Kaibuchi, S. Kuroda, M. Ui, H. Iba, H. Konishi, et al. 1997. Expression of a constitutively active phosphatidylinositol 3-kinase induces process formation in rat PC12 cells. *J. Biol. Chem.* 272:16089–16092.

Lee, C.H., N.G. Della, C.E. Chew, and D.J. Zack. 1996. Rin, a neuron-specific and calmodulin-binding small G-protein, and Rit define a novel subfamily of Ras proteins. *J. Neurosci.* 16:6784–6794.

Li, Z., L.V. Aelst, and H.T. Cline. 2000. Rho GTPases regulate distinct aspects of dendritic arbor growth in *Xenopus* central neurons in vivo. *Nat. Neurosci.* 3:217–225.

Lim, L., E. Manser, T. Leung, and C. Hall. 1996. Regulation of phosphorylation pathways by p21 GTPases. *Eur. J. Biochem.* 242:171–185.

Lindenbaum, M.H., S. Carbonetto, F. Grosveld, D. Flavell, and W.E. Mushynski. 1988. Transcriptional and post-transcriptional effects of nerve growth factor on expression of the three neurofilament subunits in PC-12 cells. *J. Biol. Chem.* 263:5662–5667.

Luo, L. 2000. Rho GTPases in neuronal morphogenesis. *Nat. Rev. Neurosci.* 1:173–180.

Mark, M.D., Y. Liu, S.T. Wong, T.R. Hinds, and D.R. Storm. 1995. Stimulation of neurite outgrowth in PC12 cells by EGF and KCl depolarization: a Ca^{2+}-independent phenomenon. *J. Cell Biol.* 130:701–710.

Marshall, C.J. 1995. Specificity of receptor tyrosine kinase signaling: transient versus sustained extracellular signal-regulated kinase activation. *Cell.* 80: 179–185.

McCormick, F. 1989. ras GTPase Activating protein: signal transmitter and signal terminator. *Cell.* 56:5–8.

Mizushima, S., and S. Nagata. 1990. pEF-BOS, a powerful mammalian expression vector. *Nucleic Acids Res.* 18:5322.

Nakayama, A.Y., M.B. Harms, and L. Luo. 2000. Small GTPases Rac and Rho in the maintenance of dendritic spines and branches in hippocampal pyramidal neurons. *J. Neurosci.* 20:5329–5338.

Poser, S., and D.R. Storm. 2001. Role of Ca^{2+}-stimulated adenylyl cyclases in LTP and memory formation. *Int. J. Dev. Neurosci.* 19:387–394.

Reuther, G.W., and C.J. Der. 2000. The Ras branch of small GTPases: Ras family members don't fall far from the tree. *Curr. Opin. Cell Biol.* 12:157–165.

Rhoads, A.R., and F. Friedberg. 1997. Sequence motifs for calmodulin recognition. *FASEB J.* 11:331–340.

Rusyn, E.V., E.R. Reynolds, H. Shao, T.M. Grana, T.O. Chan, D.A. Andres, and A.D. Cox. 2000. Rit, a non-lipid-modified Ras-related protein, transforms NIH3T3 cells without activating the ERK, JNK, p38 MAPK or PI3K/Akt pathways. *Oncogene.* 19:4685–4694.

Shao, H., K. Kadono-Okuda, B.S. Finlin, and D.A. Andres. 1999. Biochemical characterization of the Ras-related GTPases Rit and Rin. *Arch. Biochem. Biophys.* 371:207–219.

Spencer, M.L., H. Shao, H.M. Tucker, and D.A. Andres. 2002. Nerve growth factor-dependent activation of the small GTPase Rin. *J. Biol. Chem.* 277: 17605–17615.

Teng, K.K., and L.A. Greene. 1993. Depolarization maintains neurites and priming of PC12 cells after nerve growth factor withdrawal. *J. Neurosci.* 13: 3124–3135.

Vojtek, A.B., and C.J. Der. 1998. Increasing complexity of the Ras signaling pathway. *J. Biol. Chem.* 273:19925–19928.

Wes, P.D., M. Yu, and C. Montell. 1996. RIC, a calmodulin-binding Ras-like GTPase. *EMBO J.* 15:5839–5848.

Wong, S.T., J. Athos, X.A. Figueroa, V.V. Pineda, M.L. Schaefer, C.C. Chavkin, L.J. Muglia, and D.R. Storm. 1999. Calcium-stimulated adenylyl cyclase activity is critical for hippocampus-dependent long-term memory and late phase LTP. *Neuron.* 23:787–798.

Zhao, Z.S., E. Manser, X.Q. Chen, C. Chong, T. Leung, and L. Lim. 1998. A conserved negative regulatory region in αPAK; inhibition of PAK kinases reveals their morphological roles downstream of Cdc42 and Rac1. *Mol. Cell. Biol.* 18:2153–2163.

Development/Plasticity/Repair

Inhibitory But Not Excitatory Cortical Neurons Require Presynaptic Brain-Derived Neurotrophic Factor for Dendritic Development, as Revealed by Chimera Cell Culture

Keigo Kohara,[1,2] Akihiko Kitamura,[1,2] Naoki Adachi,[1,2] Megumi Nishida,[1,2] Chiaki Itami,[3] Shun Nakamura,[3] and Tadaharu Tsumoto[1,2]

[1]Division of Neurophysiology, Osaka University Graduate School of Medicine, Suita 565-0871, Japan, [2]Core Research for Evolutional Science and Technology, Japan Science and Technology Corporation, Kawaguchi 442-0012, Japan, and [3]Division of Biochemistry and Cellular Biology, National Institute of Neuroscience, Kodaira 187-8502, Japan

To address questions of whether endogenous BDNF acts differentially on inhibitory and excitatory neurons, and through what routes, we used chimera culture of cerebral cortical neurons derived from *BDNF−/−* mice and another type of transgenic mice that express green fluorescence protein and BDNF. Presynaptic BDNF transferred to both types of neurons, GABA-synthesizing enzyme-positive and -negative neurons. The latter neurons were confirmed to be glutamatergic with immunocytochemistry. Dendritic development of the former inhibitory neurons was promoted by endogenous BDNF transferred from presynaptic, excitatory neurons. In contrast, dendritic development of excitatory neurons was not related to the presence or absence of presynaptic BDNF, suggesting that BDNF acts on inhibitory neurons through an anterograde, transsynaptic route so as to promote dendritic development, whereas this is not the case in excitatory neurons.

Key words: neurotrophin; brain-derived neurotrophic factor; dendritic growth; inhibitory neuron; visual cortex; chimera cell culture; green fluorescence protein

Introduction

Brain-derived neurotrophic factor (BDNF) is known to play a crucial role in development and plasticity of neuronal circuits in the CNS (for review, see Thoenen, 1995; McAllister et al., 1999; Bibel and Barde, 2000; Poo, 2001). In addition to actions on dendritic growth of pyramidal neurons in visual cortex (McAllister et al., 1995, 1996, 1997; Horch et al., 1999), BDNF has been reported to regulate development of inhibitory neurons containing GABA in the brain. For example, BDNF promotes the phenotype differentiation of GABAergic neurons in hippocampus and striatum (Ip et al., 1993; Nawa et al., 1993; Mizuno et al., 1994; Marty et al., 1996; Ivkovic and Ehrlich, 1999; Yamada et al., 2002), facilitates dendritic development of hippocampal GABAergic neurons in culture (Bartrup et al., 1997; Vicario-Abejon et al., 1998), increases the density of inhibitory synapses (Marty et al., 2000) or the size of inhibitory terminals (Bolton et al., 2000) of hippocampal neurons, and plays a role in activity-dependent regulation of inhibition at cortical and hippocampal synapses (Rutherford et al., 1997; Tanaka et al., 1997; Frerking et al., 1998). Furthermore, depletion and overexpression of BDNF in transgenic mice impairs dendritic growth of cerebellar Purkinje cells (Schwartz et al., 1997) and accelerates maturation of GABAergic neurons in visual cortex (Huang et al., 1999), respectively.

Because these results were obtained with exogenously applied BDNF or with the nonphysiological level of BDNF, however, an important question of whether endogenous BDNF in the physiological condition exerts such an action is not answered yet. Also, a route through which endogenous BDNF acts on inhibitory neurons is not clarified, although glutamatergic or catecholaminergic neurons were suggested to be a source of BDNF (Nawa et al., 1995; Altar et al., 1997; Marty et al., 1997; Fawcett et al., 2000). Furthermore, another question of whether endogenous BDNF acts on inhibitory neurons in a different way from its action on excitatory neurons has not explicitly been answered yet.

To address these questions, we took an advantage of neurons derived from BDNF knock-out mice, because in these neurons one can detect an uptake of endogenous BDNF from other neurons of wild-type mice if both types of neurons are cocultured. In this preparation, however, it is practically difficult to differentiate neurons of knock-out mice from those of wild-type mice, because BDNF can be transferred from cell to cell. To overcome this problem, we prepared a mixed cell culture with another type of transgenic mice in which all the cells express green fluorescence protein (GFP) (Okabe et al., 1997; Fujikawa et al., 2000). In this chimera culture of neurons prepared from the different types of

Received Oct. 9, 2002; revised April 21, 2003; accepted April 23, 2003.

This work was supported by a grant-in-aid for Scientific Research on Priority Areas–Advanced Brain Science Project from the Ministry of Education, Science, Sports and Culture of Japan (T.T.). We express many thanks to Drs. M. Okabe, R. Katoh-Semba, T. Kaneko, T. Torashima, Y. Hata, and K. Souya for providing GFP mice, anti-BDNF antibody, anti-glutaminase antibody, and technical advices of immunostaining, drawing neuronal dendrites, and confocal microscopy, respectively.

Correspondence should be addressed to Dr. Tadaharu Tsumoto, Division of Neurophysiology (D-14), Osaka University Graduate School of Medicine, 2-2 Yamadaoka, Suita 565-0871, Japan. E-mail: ttsumoto@nphys.med.osaka-u.ac.jp.

 0270-6474/03/236123-09$15.00/0

transgenic mice, we could unambiguously identify neurons having the potential to express endogenous BDNF with GFP tag and those lacking the potential under a fluorescence microscope. Combined with immunocytochemistry with antibody to GABA-synthesizing enzyme, we found that GABAergic neurons require BDNF of presynaptic, excitatory neurons for development of their dendrites, but excitatory neurons do not require such presynaptic BDNF.

Materials and Methods

Chimera culture of neurons. Neonatal GFP mice (C57BL/6; provided by Dr. M. Okabe, Genome Information Research Center, Osaka University, Suita 565-0871, Japan) and mice (C57BL/6; provided by Regeneron Pharmaceuticals, Tarrytown, NY) that were confirmed to be *BDNF−/−* mice with genotyping were anesthetized with ketamine (>30 mg/kg, i.p.) and then killed by cervical dislocation at postnatal days 2–3. Genotyping of neonatal mice was performed in the same way as described previously (Itami et al., 2000). The experimental procedures met the regulation of the Animal Care Committee of Osaka University Graduate School of Medicine. Neurons derived from *BDNF−/−* and GFP mice were cultured on the same glial feeder layers that had been prepared previously from *BDNF−/−* mice. The density of GFP and *BDNF−/−* neurons were 25–50 cells/cm^2 and ~1000 cells/cm^2, respectively. The detailed method of culturing neurons was described previously (Kohara et al., 2001). All experiments were performed 14–21 d after plating. In part of the experiments, anti-BDNF antibody (30 μg/ml; Promega, Madison, WI) was added to the culture medium at 2 d after plating to neutralize endogenous BDNF.

Injection of plasmid cDNA of DsRed or Neurobiotin. In part of the experiments, plasmid cDNAs of DsRed (DsRed-Express; Clontech, Palo Alto, CA) were injected into the nucleus of neurons through micropipettes at the concentration of 1 μg/μl to trace axons of the neurons under observation. Axon terminals of injected neurons were visualized, as reported previously (Kohara et al., 2001). In another series of the experiments, 10% *N*-(2-aminoethyl)biothinamide hydrochloride (Neurobiotin;Vector Laboratories, Burlingame, CA) in PBS was injected into neurons through micropipettes. Neurobiotin was visualized by NeutrAvidin conjugated Alexa 350 (1: 1000; Molecular Probes, Eugene, OR).

Immunocytochemistry. For immunocytochemical staining, neurons were fixed usually with 4% paraformaldehyde (PFA; Sigma, St. Louis, MO) and 4% sucrose in PBS, pH 7.0, for 30 min at room temperature. For analysis of dendritic morphology, neurons were fixed with 4% PFA and 4% sucrose in PBS, pH 7.4, for 20 min at room temperature. The cells were incubated with PBS containing 0.2% Triton-X (Sigma) for 1 min and blocked by 10% goat serum in PBS for 1 hr at 37°C. Then, anti-MAP2 monoclonal antibody (isotype:IgG1, 1:250; Sigma), anti-synaptotagmin monoclonal antibody (isotype:IgG2b, 1:200; Calbiochem, San Diego, CA), anti-GAD65 monoclonal antibody (isotype:IgG2a, 1:1000; Chemicon, Temecula, CA), anti-BDNF rabbit polyclonal antibody (2 μg/ml; provided by Dr. R. Katoh-Semba, Institute for Developmental Research, Kasugai 480-0392, Japan) (Katoh-Semba et al., 1997, 2001), anti-GFP chicken polyclonal antibody (1:1000; Chemicon), or anti-GFP rabbit polyclonal antibody (1:1000; Molecular Probes) was applied for 2 hr at 37°C. MAP2, synaptotagmin, and GAD65 were visualized by isotype-specific secondary antibody conjugated with Alexa 350 (1:200; Molecular Probes), Alexa 546 (1:2000), and Alexa 647 (1:200). GFP and BDNF were visualized by anti-chicken secondary antibody conjugated with Alexa 488 (1:1000) and anti-rabbit secondary antibody conjugated with Cy5 (1: 200; Chemicon). GFP has its own fluorescence but it is gradually fading during observation. Once GFP is immunocytochemically stained with anti-GFP antibody, however, the fluorescence does not fade so quickly. Therefore, immunocytochemical staining of GFP was necessary for observation of neurites of neurons. Fluorescent signals were observed with a 40×/1.3 numerical aperture oil immersion objective (Plan Flour; Nikon, Tokyo, Japan) attached to an inverted epifluorescence microscope and captured by a cooled CCD camera (C4742–95; Hamamatsu Photonics, Hamamatsu, Japan). This system consisted of 1024 × 1024 pixels, each of which corresponded to 0.17 × 0.17 μm with the 40× objective. Filters (UV2EC, B2EC, and G2EC; Nikon; XF110; Omega Optical, Brattleboro, VT) were used for four-color immunofluorescence detection. Fluorescence data were analyzed further with an Aquacosmos system (Hamamatsu Photonics). In part of the experiments, a confocal fluorescence microscope (E600FN; Nikon; Radiance 2000; Bio-Rad, Hercules, CA) was used to obtain thin-sliced images of stained neurons.

Measurement of fluorescent signal. The fluorescence intensity of BDNF was measured on a square window (30 × 30 pixels; 5.1 × 5.1 μm) placed on the soma of a neuron under observation, and the mean fluorescence intensity of 900 pixels was calculated by subtracting the noise of the CCD camera system that was detected in the complete darkness. The window was placed randomly on the soma in the blind condition, i.e., the window was placed by an experimenter who had not seen any BDNF image of the neuron, and then the fluorescence intensity was measured automatically by the Aquacosmos system. As control, the soma of another neuron that was not contacted by GFP-positive terminals was randomly selected in the same culture dish. The intensity of fluorescence in such a control neuron was calculated in the same way as above. Because the soma of control neurons had some background fluorescence, its fluorescence intensity was expressed as 100%, and that of test neurons was normalized to this value.

Analysis of morphology. After immunocytochemical staining, neurons, the dendrites of which did not overlap with dendrites of other neurons, were randomly selected from the same dishes. After having recorded fluorescent images, neurons were incubated with anti-mouse IgG1-conjugated biotin for 1 hr at 37°C. Then, an ABC kit (Vector Laboratories) was used for visualization of MAP2. Neurolucida (MicroBrightField, Williston, VT) attached to an upright microscope (E600; Nikon) was used for drawing dendrites of neurons. The quantitative assessment of dendritic morphology was done with an analyzing software, Neuroexplore (MicroBrightField).

Results

Transfer of endogenous BDNF from presynaptic terminals to postsynaptic neurons

We prepared chimera culture of cortical neurons from homozygously knock-out mice of BDNF gene (*BDNF−/−* mice) and from GFP mice (Fig. 1*A*). In this culture, GFP-positive neurons are expected to have the potential to express endogenous BDNF, whereas GFP-negative neurons are not. In fact, we confirmed that the former neurons expressed endogenous BDNF in a punctuated manner in neurites (Fig. 1*B*, *C*), whereas the latter neurons did not have any sign of endogenous BDNF (Fig. 1*E*, *F*). Such a GFP-negative neuron became visible by immunocytochemistry with antibody to MAP2, which is a marker of somatodendritic region of neurons (Fig. 1*G*).

To identify GABAergic neurons, we stained neurons with antibody to GAD65, which is known to be a synthesizing enzyme of GABA in presynaptic terminals (Erlander and Tobin, 1991). With this immunocytochemistry, we could unambiguously detect GABAergic neurons. Then, we found that endogenous BDNF transferred from presynaptic terminals to postsynaptic GABAergic neurons. An example of this finding is shown in Figure 2. As shown in Figure 2*A*, axon branches of a GFP-positive neuron (*BDNF+/+*), the soma of which was outside the frame of this picture, made a net-like terminal arborization, which surrounded and contacted a MAP2-positive neuron (red). This postsynaptic neuron was confirmed to be a GABAergic neuron, because the immunoreactivity to antibody against GAD65 was clearly seen in its cell body (Fig. 2*B*, arrowhead). As shown in Figure 2*A*, this neuron was GFP negative and, thus, judged as derived from a BDNF knock-out mouse. In Figure 2*B*, neurites containing GAD65-positive puncta or varicosities were seen around the soma of the GABAergic neuron. These neurites were judged to be axon branches of this and other GABAergic neurons, because they were not stained with anti-MAP2 antibody (Fig. 2*A*). The superimposed picture in Figure 2*C* indicates that GFP-

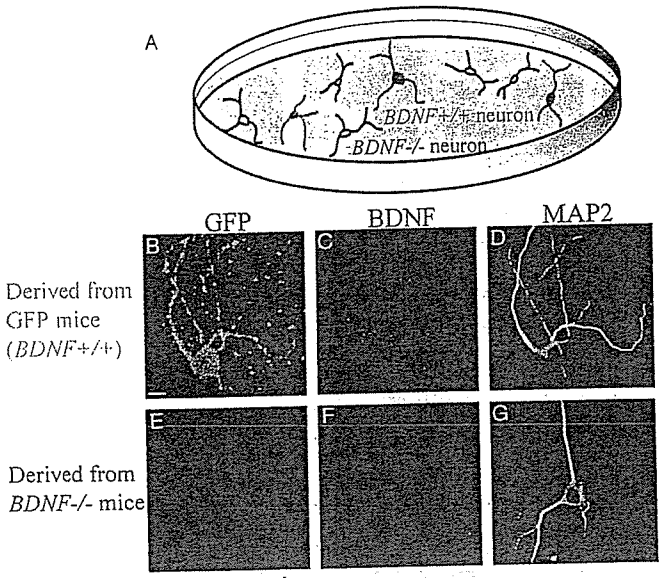

Figure 1. Chimera cell culture prepared from two types of transgenic mice. *A*, Schematic illustration of chimera culture of cortical neurons derived from *BDNF−/−* and GFP mice. The latter neurons were labeled with GFP and had the potential to express endogenous BDNF (*BDNF+/+*). *B*, GFP image of a cortical neuron derived from a GFP mouse. *C*, Immunocytochemical BDNF image of the neuron shown in *B*. *D*, MAP2 image of the neuron shown in *B* and *C*. *E*, No GFP fluorescence signal in a cortical neuron derived from a *BDNF−/−* mouse was observed. This neuron was located in the same dish as above. *F*, No BDNF immunoreactivity in the neuron shown in *E* was observed. *G*, MAP2 image of the neuron shown in *E* and *F*. Scale bar: (in *B*) *B–G*, 10 μm.

positive axon branches were GAD65 negative and, thus, not GABAergic. In Figure 2 *D*, *E*, it is seen that BDNF-positive puncta were located in presynaptic axon branches. Also, we found that the soma of the GABAergic neuron contained BDNF (Fig. 2 *D*, *E*, arrows). This suggests that endogenous BDNF was transferred from the presynaptic, GFP-positive axon branches to the postsynaptic GABAergic neuron, because this postsynaptic neuron was derived from a *BDNF−/−* mouse and, thus, should not produce endogenous BDNF by itself.

There is a possibility that BDNF signals that were detected in the soma region of neurons might be located in the pericellular space that was foreground or background of the soma. To minimize such a possibility, a very thin section (1.2 μm thick) of image was obtained with a confocal microscope in part of the experiments. As indicated by arrows in Figure 3 *B–D*, BDNF signals were seen in the soma of a postsynaptic neuron. Also, it was seen that the BDNF signals in the soma were not overlapped with GFP signals, whereas those in neurites were mostly overlapped (Fig. 3 *C*,*D*). These results confirmed that BDNF was present in the soma of the postsynaptic neuron.

To quantify the transfer of BDNF to postsynaptic neurons, the intensity of fluorescence was measured in the soma of the neurons that were contacted by GFP-positive axon terminals (Fig. 2 *F*, insets). As control, the soma of another neuron that was not contacted by GFP-positive terminals was randomly selected in the same culture dish. Because the soma of control neurons had some background fluorescence, its fluorescence intensity was expressed as 100%, and that of test neurons was normalized to this value. The mean fluorescence intensity of the somata of 10 GABAergic neurons that were contacted by GFP-positive axons was 135.0 ± 8.5% (mean ± SEM), which was significantly ($p < 0.01$; unpaired *t* test) larger than that of the seven control neurons (Fig. 2 *F*). This indicates that the postsynaptic GABAergic neuron contains endogenous BDNF that has probably been transferred from GFP-positive, *BDNF+/+* presynaptic axons.

There is a possibility that BDNF detected in the soma of GABAergic neurons might be transferred retrogradely from a GFP-positive neuron. To test such a possibility, we visualized 6 GABAergic neurons with the method of direct intranuclear injection of plasmid cDNAs of DsRed fluorescent protein (Kohara et al., 2001) and another 10 GABAergic neurons with the method of intracellular injection of a tracer, Neurobiotin. With either method, we could trace axons of the neurons until their terminals. Because we did not find a notable difference in visualization of neurons between these two methods, the data were combined. Altogether, six neurons were contacted by GFP-positive afferents. Axon terminals of three neurons contacted GFP-positive, excitatory neurons, and the other three did not. Ten GABAergic neurons were not contacted by GFP-positive afferents. Axon terminals of five of these neurons contacted GFP-positive, excitatory neurons, and those of the other five did not. It is to be noted that the former five neurons that had the possibility to receive BDNF only through the retrograde route did not have detectable BDNF signal in their cell bodies. To quantify these results, the background fluorescence intensity of the soma of the former five neurons was compared with that of the latter five neurons that had no possibility to receive BDNF through either route. The mean fluorescence intensity of the former neurons was 95.9 ± 4.1% of that of the latter neurons. The difference was insignificant (unpaired *t* test; $p > 0.05$). Thus, these results suggest that the possibility of retrograde transport is negligible in our preparations, although we cannot completely exclude such a mechanism.

An intercellular transfer of endogenous BDNF in the anterograde direction was detected also in GAD65-negative neurons that were most likely excitatory neurons. In part of the experiments, neurons were immunocytochemically stained with antibody to phosphate-activated glutaminase, which is glutamate-synthesizing enzyme in the transmitter pool of cortical neurons (Kaneko and Mizuno, 1988). We observed that all of the GAD65-negative neurons were reactive to this antibody, indicating that GAD65-negative neurons were glutamatergic neurons. The mean fluorescence intensity of the somata of 16 GAD65-negative neurons that were contacted by GFP-positive axons was 154.8 ± 16.3% of that of another 14 GAD65-negative neurons that were not contacted by GFP-positive axons. The difference was statistically significant ($p < 0.01$; unpaired *t* test). These results indicate that presynaptic endogenous BDNF transferred to both inhibitory and excitatory neurons.

Then, we tested whether BDNF actually exists in presynaptic axon terminals. For this, we stained neurons immunocytochemically with antibody against a presynaptic marker protein, synaptotagmin (Fig. 4 *E*). Some BDNF signals were localized in GFP-positive axons, so that they appeared to be yellow puncta (Fig. 4 *C*, arrows). As shown in Figure 4 *F*, such clusters of BDNF-positive puncta were mostly colocalized with synaptotagmin-positive presynaptic terminals.

Promoted growth of dendrites of GABAergic neurons by presynaptic BDNF

To assess actions of endogenous BDNF on postsynaptic GABAergic neurons, we quantitatively analyzed the dendritic morphology of neurons that were derived from *BDNF−/−* mice. As shown in Figure 5, the dendritic morphology of neurons that were immunoreactive to anti-GAD65 antibody (Fig. 5 *B*,*E*) was visualized by immunocytochemistry with anti-MAP2 antibody

(Fig. 5*A*,*D*). The neuron shown in Figure 5*A* was contacted by GFP-positive (*BDNF*+/+) axon terminals, as shown by yellow puncta in Figure 5*C*, in which the picture stained with anti-GFP antibody (green) was superimposed with that with anti-synaptotagmin antibody (red). The neuron shown in Figure 5*D* was contacted by GFP-negative axon terminals that were shown by synaptotagmin-postive puncta (*F*). In Figure 5*A*,*D*, it is obvious that the GABAergic neuron contacted by GFP-positive (*BDNF*+/+) terminals had much more abundant dendritic branches than the other neuron contacted by GFP-negative axons (*BDNF*−/−). The total picture of dendrites of another pair of GABAergic neurons is shown in Figure 6*A*. Again, it is obvious that the neuron contacted by GFP-positive (*BDNF*+/+) terminals had well developed dendrites (right), whereas that contacted by GFP-negative axons (*BDNF*−/−) had relatively poor dendrites (left).

To quantify this finding, we calculated three parameters of dendritic morphology of each neuron (Fig. 7). The mean total length of dendrites of 14 GABAergic neurons that were contacted by GFP-positive axons (*BDNF*+/+) and that of other 12 GABAergic neurons that were contacted by GFP-negative axons (*BDNF*−/−) were 2376.7 ± 225.5 μm and 1345.2 ± 152.9 μm, respectively (Fig. 7*A*, left two columns). The difference between these two values was statistically significant ($p < 0.01$; ANOVA). The mean numbers of dendritic branch points of the neurons contacted by GFP-positive and GFP-negative axons were 22.2 ± 2.0 and 13.3 ± 1.9, respectively (Fig. 7*B*, left two columns). The difference between these two values was, again, significant ($p < 0.01$; ANOVA). In contrast, the number of primary dendrites was not affected by presynapic BDNF (Fig. 7*C*, left two columns). The mean numbers of primary dendrites of the neurons contacted by GFP-positive and GFP-negative axons were 7.0 ± 0.5 and 6.2 ± 0.6, respectively. These results suggest that endogenous BDNF, which probably was supplied from presynaptic terminals, may promote branch formation of dendrites of postsynaptic GABAergic neurons.

To confirm that such an effect of contact with GFP-positive (*BDNF*+/+), presynaptic terminals was induced by extracellularly released BDNF, we applied anti-BDNF antibody, which blocks function of BDNF, to chimera culture preparations. As shown in Figure 6*B* (right), a GABAergic neuron cultured with anti-BDNF antibody had relatively poor dendrites even when it was contacted by GFP-positive (*BDNF*+/+) terminals. The complexity of their dendritic arborization seemed to be about the same as that of another GABAergic neuron that was contacted by GFP-negative axons (*BDNF*−/−) (Fig. 6*B*, left). This is seen in the quantitative analysis of the three parameters of dendrites (Fig. 7*A–C*, right two columns). The mean total lengths of dendrites of the two groups of GABAergic neurons that were treated with anti-BDNF antibody were 1177.8 ± 149.5 μm and 1173.9 ± 209.8 μm, respectively (Fig. 7*A*, right two columns; $n = 8$ and 9, respectively). The mean numbers of dendritic branch points of the two groups of neurons were 13.0 ± 1.1 and 12.0 ± 2.2, re-

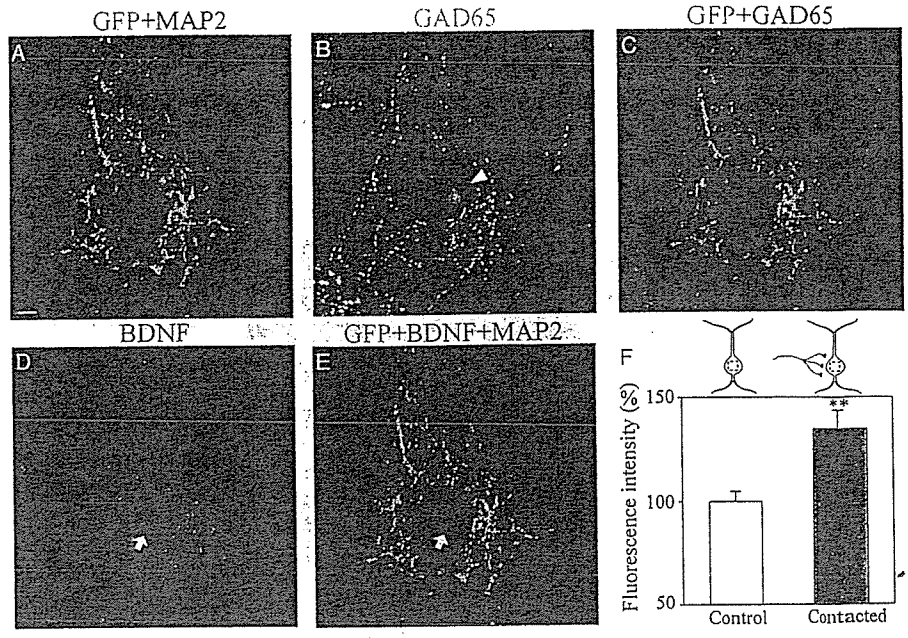

Figure 2. Transfer of endogenous BDNF to postsynaptic GABAergic neurons. *A*, Superposition of GFP image (green) and MAP2 image (red) of cultured neurons. A GFP-negative postsynaptic neuron (red) was contacted by GFP-positive axon branches and their terminals (green). Scale bar, 10 μm. *B*, GAD65 image of the same frame as in *A*. The arrowhead indicates the soma. *C*, Superposed image of GFP signals (green) and GAD65 signals (red). *D*, Endogenous BDNF image of the same frame as the others. The arrow indicates the soma of the postsynaptic neuron. *E*, Superposed image of GFP signals (green), BDNF signals (red), and MAP2 signals (blue). *F*, Mean value of intensity of BDNF signal in two groups of neurons. The top schematically shows the method to measure the fluorescence intensity of BDNF signal in neurons. The mean values obtained from GABAergic neurons that did not contact GFP-positive terminals (□) and contacted such terminals (■). Vertical bars indicate SEM. Double asterisks indicate statistical significance of the difference from the control at $p < 0.01$ (unpaired *t* test).

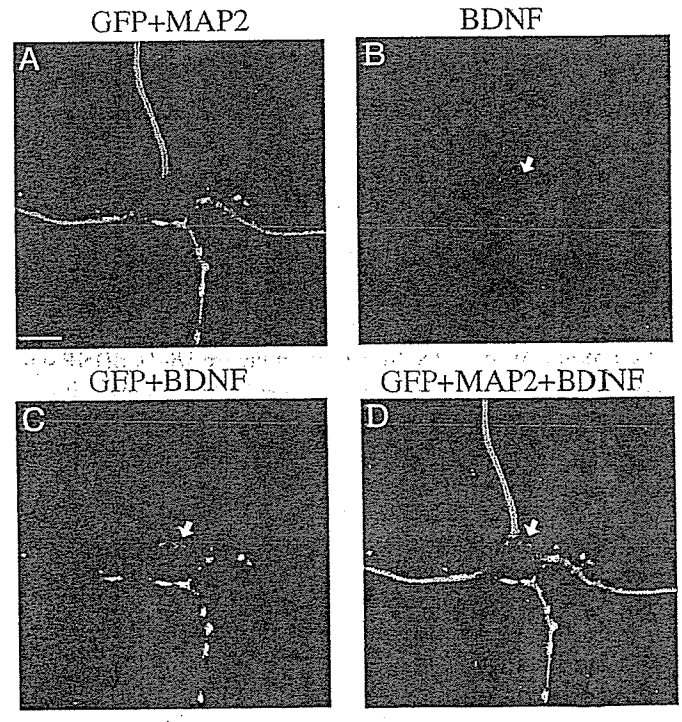

Figure 3. Intraneuronal BDNF visualized by confocal microscopy. All pictures were single focal sections of 1.2 μm thickness. *A*, Superposed image of GFP signals (green) and MAP2 signals (blue). *B*, BDNF image (red) of the same frame as *A*. The arrow shows BDNF signals in the cell body. *C*, Superposed image of GFP and BDNF. BDNF signal in the cell body (arrow) was not superposed with GFP-positive neurites. *D*, Superposed image of GFP, MAP2, and BDNF. Scale bar: (in *A*) 10 μm.

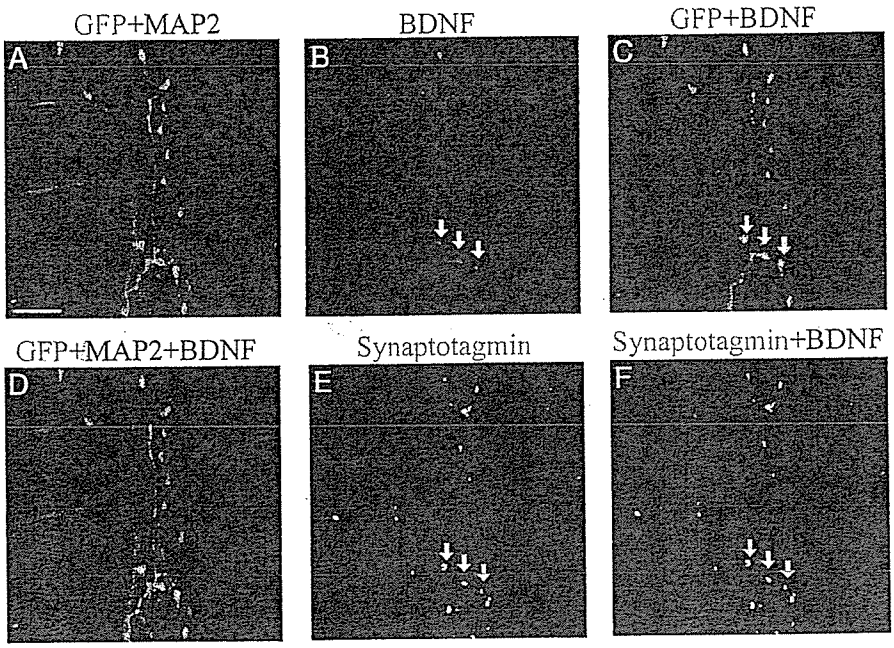

Figure 4. Existence of endogenous BDNF in presynaptic axon terminals. *A*, Superposed image of GFP signals (green) and MAP2 signals (blue). *B*, BDNF image (red) of the same frame as *A*. The arrows show clusters of BDNF signals. Faint BDNF signal was seen in the soma of the postsynaptic neuron, as shown in *D*. *C*, Superposed image of GFP and BDNF. BDNF puncta were colocalized with GFP-positive neurites (arrows). *D*, Superposed image of GFP, MAP2, and BDNF. *E*, Synaptotagmin image of the same frame as the others. The arrows indicate the same puncta as in *B*, *C*, and *F*. *F*, Superposed image of synaptotagmin (blue) and BDNF (red). BDNF puncta indicated by arrows were colocalized with synaptotagmin. Scale bar: (in *A*) 10 μm.

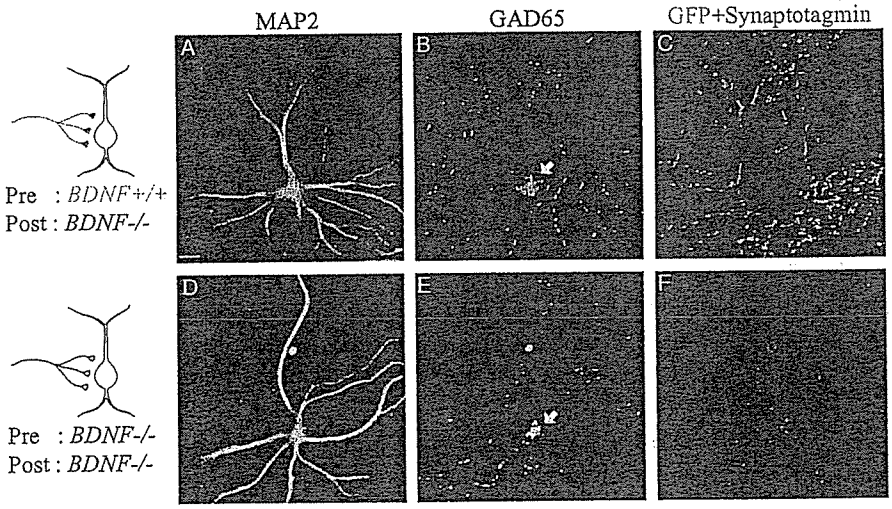

Figure 5. Promoted growth of dendrites of GABAergic neurons by presynaptic BDNF. *A*, MAP2 image of a neuron contacted by a GFP-positive axon (*BDNF*+/+), as schematically shown on the left. *B*, GAD65 image of the same frame as in *A*. The arrow shows the cell body. *C*, Superposition of GFP images (green) and synaptotagmin images (red) of the same frame as *A* and *B*. *D*, MAP2 image of a neuron contacted by a GFP-negative axon (*BDNF*−/−), as schematically shown on the left. *E*, GAD65 image of the same frame as in *D*. The arrow shows the cell body. *F*, Superposition of GFP images (green) and synaptotagmin images (red) of the same frame as *D* and *E*. Because both the presynaptic and postsynaptic neurons were GFP negative, there was no green signal. Scale bar: (in *A*), 10 μm.

spectively (Fig. 7*B*, right two columns). The mean numbers of primary dendrites of the two groups of neurons were 6.1 ± 0.5 and 5.4 ± 0.7, respectively (Fig. 7*C*, right two columns). In any of these three parameters, there was no significant difference between the two groups of GABAergic neurons, to which anti-BDNF antibody was applied.

In this quantitative analysis, it is also seen that the total length of dendrites and the number of dendritic branch points of the GABAergic neurons that were contacted by GFP-negative afferents were not reduced by the treatment with the anti-BDNF antibody (Fig. 7*A*,*B*, compare the third columns with the leftmost columns). There was no statistically significant difference (unpaired *t* test; $p > 0.05$) between these two columns in any of the three parameters (Fig. 7).

No effect of presynaptic BDNF on dendritic growth of excitatory neurons

Finally, we examined effects of presynaptic BDNF on the dendritic morphology of GAD65-negative neurons and found that the presence or absence of presynaptic BDNF is not related to dendritic growth of such excitatory neurons. Examples of GAD65-negative neurons are shown in Figure 8. The GAD65 negativity was obvious, in particular, in their somata (Fig. 8*B*,*E*, arrows), although the neuron in Figure 8*B* seemed to be surrounded by GAD65-positive puncta that were assumed to be GABAergic axon terminals. These neurons were judged as derived from *BDNF*−/− mice, because they were GFP negative (Fig. 8*C*,*F*). The seemingly yellow staining of some regions of the neuron shown in Figure 8*F* was because of GFP-positive presynaptic terminals, the soma of which was outside the frame of this picture. As seen in Figure 8*A*,*D*, the extent of dendritic arborization of the BDNF-negative excitatory neuron contacted by a GFP-positive axon (*BDNF*+/+) (Fig. 8*D*) was about the same as that of the neuron contacted by a GFP-negative axon (*BDNF*−/−) (Fig. 8*A*).

The dendritic morphology of these two groups of excitatory neurons that were derived from (*BDNF*−/−) mice was analyzed in the same way as in Figure 7 (Fig. 8*G*–*I*). The total length of dendrites of 17 excitatory neurons contacted by GFP-positive axons (1181.5 ± 123.1 μm) was not significantly (unpaired *t* test; $p > 0.05$) different from that of another 16 excitatory neurons contacted by GFP-negative axons (998.1 ± 120.0 μm) (Fig. 8*G*). The mean numbers of dendritic branch points (11.1 ± 1.6) and primary dendrites (4.6 ± 0.3) of the excitatory neurons with GFP-positive axons were not significantly different from those of the neurons with GFP-negative axons (10.1 ± 1.5 and 4.9 ± 0.5, respectively) (Fig. 8*H*,*I*) (unpaired *t* test; $p > 0.05$). Thus, the presence or absence of presynaptic BDNF had no effects on dendritic development of postsynaptic, excitatory neurons.

Discussion

It is well established that GABAergic neurons do not have mRNA of BDNF and, thus, cannot produce BDNF by themselves (Ernfors et al., 1990; Cellerino et al., 1996; Rocamora et al., 1996;

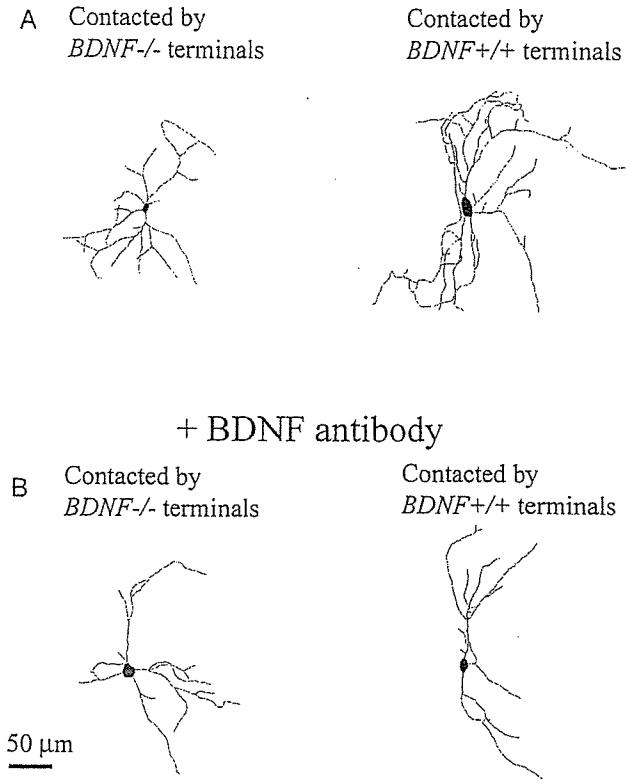

Figure 6. Morphology of dendrites of GABAergic neurons and effects of anti-BDNF antibody. *A*, Left, Dendritic morphology of a GABAergic neuron (*BDNF−/−*) that was contacted by GFP-free (*BDNF−/−*) axons. Right, Dendritic morphology of another GABAergic neuron (*BDNF−/−*) that was contacted by GFP-positive (*BDNF+/+*) axons. *B*, Dendritic morphology of GABAergic neurons (*BDNF−/−*) treated with anti-BDNF antibody. Left and right, Neurons were contacted by GFP-free axons (*BDNF−/−*) and GFP-positive axons (*BDNF+/+*), respectively.

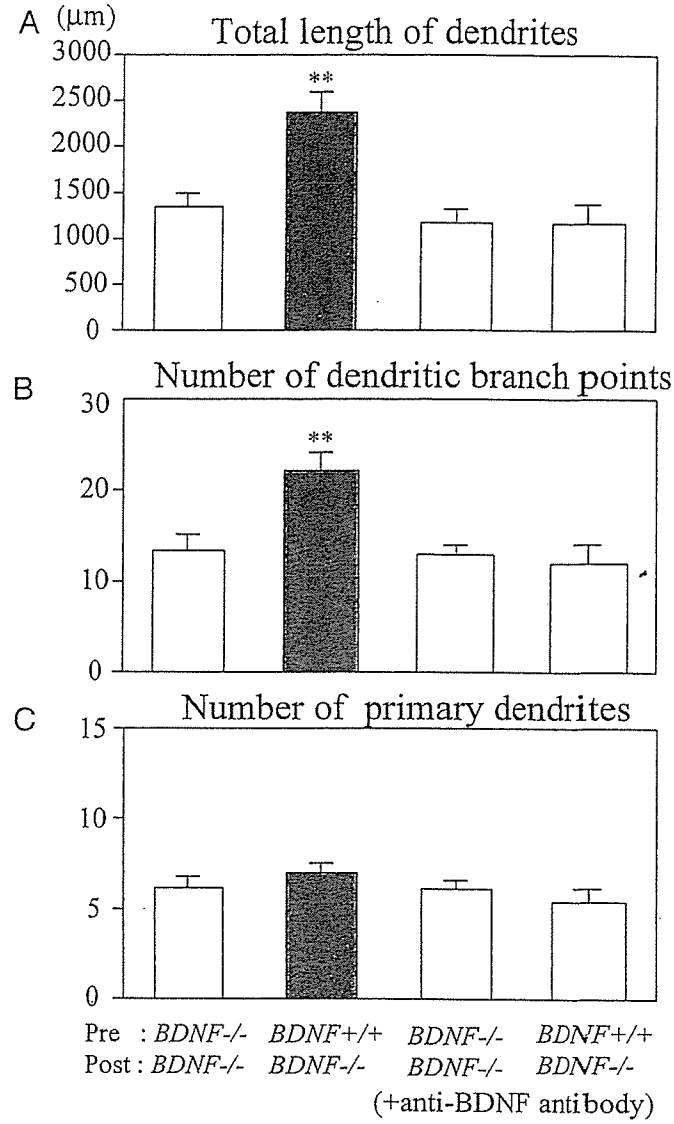

Figure 7. Quantitative assessment of actions of presynaptic BDNF on dendrites of GABAergic neurons. *A*, Mean values of the total length of dendrites of neurons contacted by GFP-negative axons (*BDNF−/−*) (leftmost column) and GFP-positive axons (*BDNF+/+*) (hatched column) in the control medium and corresponding values of neurons treated with anti-BDNF antibody (third and rightmost columns). Vertical bars indicate SEM. Double asterisks in *A* and *B* indicate statistical significance of the difference at $p < 0.01$ (ANOVA). *B*, Mean number of dendritic branch points per neuron. *C*, Mean number of primary dendrites per neuron. In *B* and *C*, neurons are grouped in the same way as in *A*.

Gorba and Wahle, 1999). In the present study, we have found that such GABAergic neurons had a clear signal of the existence of BDNF in their cell bodies. This BDNF is judged to have been transferred from presynaptic GFP-positive axons that contain endogenous BDNF, because only the GABAergic neurons that were contacted by GFP-positive axon terminals had significant signals, but those that were not contacted by such terminals had not. A previous report also suggested that interneurons could incorporate BDNF that might be released from pyramidal cells in rat hippocampus (Schmidt-Kastner et al., 1996). However, they did not show that their interneurons were GABAergic and also did not provide direct evidence that BDNF was actually transferred to those neurons from pyramidal neurons.

The present study further indicates that BDNF that has been transferred in such a way promotes dendritic development of GABAergic neurons, because the neurons contacted by GFP-positive axon terminals had well developed dendrites, but those not contacted by such terminals had relatively poor dendrites. The better development of dendrites of the former neurons is thought to result from intercellularly transferred BDNF, because anti-BDNF antibody that was applied through the culture medium and, thus, expected to neutralize BDNF in the extracellular space blocked such a proliferous action.

There is a possibility that GABAergic neurons might receive BDNF through their axons from GFP-positive, postsynaptic neurons and such target-derived BDNF might exert the proliferous action, because BDNF is known to be transported also retrogradely from postsynaptic neurons to presynaptic axon terminals (Causing et al., 1997; Marty et al., 1997; Watson et al., 1999). This possibility seems unlikely, however, for two reasons. First, in the present study, none of the GABAergic neurons that did not receive GFP-positive afferents but sent their axons to other GFP-positive, excitatory neurons had detectable BDNF signal in their cell bodies. If endogenous BDNF is transferred in the retrograde direction, we should have detected BDNF signal in such GABAergic neurons. Second, if target-derived BDNF has some effects on GABAergic neurons, the functional block of released BDNF by the anti-BDNF antibody should have affected dendritic development of the GABAergic neurons that were contacted by GFP-negative terminals. The results shown in Figure 7 indicate, however, that the application of the antibody did not exert significant

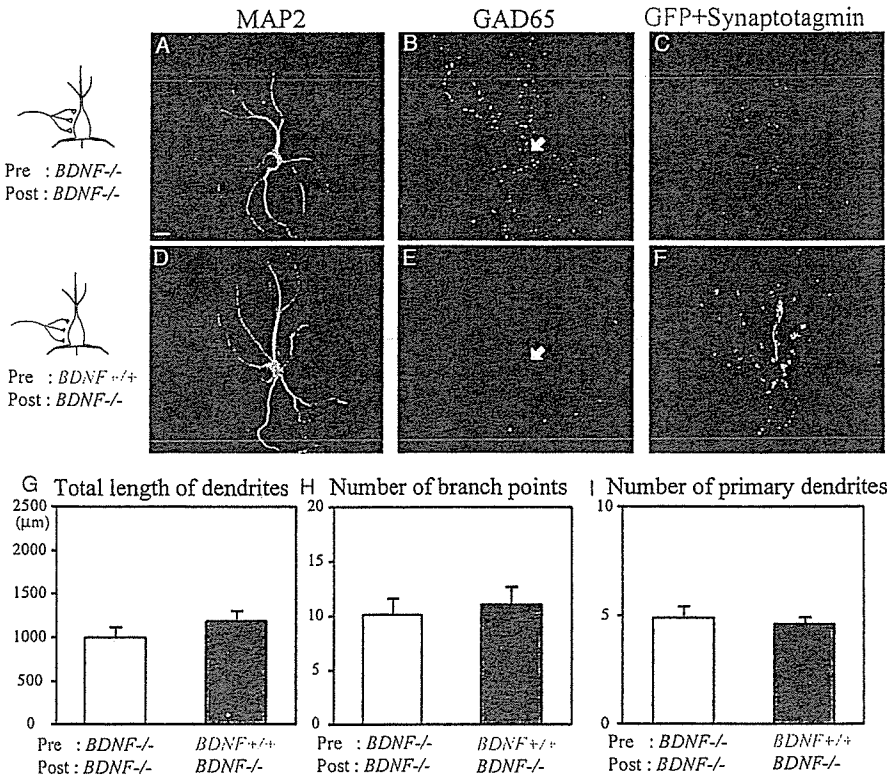

Figure 8. No effect of presynaptic BDNF on growth of dendrites of excitatory neurons. *A*, *D*, MAP2 images of a *BDNF−/−* neuron that was contacted by *BDNF−/−* axons and *BDNF+/+* axons, respectively. *B*, *E*, GAD65 images of the neurons shown in *A* and *D*, respectively. The arrows indicate the location of the soma. Note the lack of label in the cell body of both neurons. *C*, *F*, Superposed image of GFP and synaptotagmin signals of the neurons shown in *A* and *D*, respectively. Scale bar: (in *A*) 10 μm. *G*, Mean value of the total length of dendrites of excitatory neurons contacted by GFP-negative axons (*BDNF−/−*) (open column) and by GFP-positive axons (*BDNF+/+*) (hatched column). Vertical bars indicate SEM. *H*, Mean number of branch points of dendrites per neuron. *I*, Mean number of primary dendrites per neuron.

actions on the dendritic development of this group of GABAergic neurons (Fig. 7*A–C*, compare the third with leftmost columns).

In the present chimera culture preparations, the densities of GFP/BDNF-positive and -negative neurons were different. If the density of the former neurons was higher than that of the latter neurons, the number of GFP/BDNF-positive terminals might have exceeded that of GFP/BDNF-negative terminals. Consequently, GABAergic neurons that were contacted by the former terminals might have developed their dendrites better simply because of the greater number of contacts, irrespectively of BDNF transfer. To minimize this possibility, we set the ratio of the density of GFP/BDNF-positive and -negative cells at 1:20–40. In this condition, the number of GFP/BDNF-positive terminals was much less than that of negative terminals. Nevertheless, GFP/BDNF-positive terminals exerted the promoting action on dendritic growth of postsynaptic GABAergic neurons. Therefore, the possibility mentioned above seems unlikely in the present preparations.

Because GABAergic neurons do not have mRNA of BDNF as mentioned previously, the transfer of BDNF from excitatory neurons may be crucial for development of dendritic arborization of GABAergic neurons. In visual cortex *in vivo*, it is known that most, if not all, GABAergic neurons are contacted by axons of pyramidal neurons (Kisvarday, 1992; Johnson and Burkhalter, 1996). Also, it is well established that neocortical pyramidal neurons express BDNF (Yan et al., 1997; Friedman et al., 1998). Thus, it seems reasonable to assume that endogenous BDNF released from pyramidal cell axons acts on GABAergic neurons in visual cortex *in vivo*. However, previous studies in hippocampal neurons suggested that BDNF transferred retrogradely from excitatory neurons to GABAergic neurons may promote growth of the latter neurons (Marty et al., 1996, 1997). The present results have demonstrated, however, that the anterograde transfer of BDNF from excitatory neurons to GABAergic neurons plays such a role, although we cannot exclude any retrograde transfer. Anterogradely transferred BDNF, then, may activate the local protein synthesis that leads to growth of dendrites of postsynaptic neurons, as suggested (Aakalu et al., 2001; Takei et al., 2001).

In excitatory neurons, the transcellular transfer of BDNF seems to be not so important in the development of their dendrites, because the dendritic development was not correlated with the existence of presynaptic BDNF. This raises a possibility that the expression of functionally active or inactive BDNF receptors such as full-length and truncated TrkB in excitatory neurons might be different from that of inhibitory neurons. To our knowledge, there was no study in which the two types of receptors were differentially stained, except for a study in which full-length TrkB and pan TrkB including truncated type were differentially stained in the hippocampal formation of adult rats (Drake et al., 1999). In this study, no marked difference was reported in localization of immunoreactivity between full-length and pan TrkBs, although the intensity of reactivity was different at various subcellular sites. Thus, a reason why transferred BDNF was less important in dendritic development of excitatory neurons is not clear in the present study. Because excitatory neurons can produce BDNF by themselves, however, it is to be noted that endogenous BDNF may act on this type of neurons, in part at least, through an autocrine loop, as suggested previously (Kokaia et al., 1993; Miranda et al., 1993; Horch et al., 1999). From the present results, it is possible to suggest that the different actions of BDNF on excitatory and inhibitory synapses that were reported previously (Rutherford et al., 1998; Schinder et al., 2000) may be executed through the distinct pathways (i.e., anterograde, transsynaptic route to GABAergic neurons and autocrine route to glutamatergic neurons).

Because the release and transcellular transfer of BDNF are known to depend on neuronal activity (Goodman et al., 1996; Balkowiec and Katz, 2000; Hartmann et al., 2001; Kohara et al., 2001; Kojima et al., 2001; Lever et al., 2001; Gartner and Staiger, 2002), the transfer of BDNF to GABAergic neurons is assumed to be activity dependent. It is suggested that maturation of GABAergic neurons regulates the beginning of the critical period during which visual cortical neurons are highly sensitive to an alteration in inputs (Hensch et al., 1998). Furthermore, an overexpression of BDNF induces a precocious critical period in mouse visual cortex probably through its action on GABAergic neurons (Hanover et al., 1999; Huang et al., 1999). Thus, it is possible to suggest that the activity-dependent transfer of endogenous

BDNF to GABAergic neurons may promote their maturation so as to play a role in the onset of the critical period of the developing visual cortex.

It was reported that another neurotrophin, NT-3, abolished the growth-promoting effect of BDNF on pyramidal neurons in slice culture preparations of visual cortex of young ferrets (McAllister et al., 1997). A question of whether NT-3 and BDNF have such an antagonist action also on GABAergic neurons should be addressed in a future study. Finally, it is to be noted that chimera culture preparations of neurons derived from different kinds of transgenic mice are a useful tool to elucidate the functional significance of a given bioactive molecule. Although conditional knock-out systems using Cre-*loxP* and specific promoter have been developed to reveal the local functions of target proteins (Tsien et al., 1996; Minichiello et al., 1999; Xu et al., 2000a,b; Iwasato et al., 2000), it is difficult to delete them from particular synapses of given neuronal circuits. In chimera cultures of neurons, in contrast, it is easy to make neuronal circuits in which particular molecules are lacking in visually identifiable circuits. In fact, we have successfully demonstrated that dendritic development of inhibitory cortical neurons is regulated by presynaptic BDNF.

References

Aakalu G, Smith WB, Nguyen N, Jiang C, Schuman EM (2001) Dynamic visualization of local protein synthesis in hippocampal neurons. Neuron 30:489–502.

Altar CA, Cai N, Bliven T, Juhasz M, Conner JM, Acheson AL, Lindsay RM, Wiegand SJ (1997) Anterograde transport of brain-derived neurotrophic factor and its role in the brain. Nature 389:856–860.

Balkowiec A, Katz DM (2000) Activity-dependent release of endogenous brain-derived neurotrophic factor from sensory neurons detected by ELISA *in situ*. J Neurosci 20:7417–7423.

Bartrup JT, Moorman JM, Newberry NR (1997) BDNF enhances neuronal growth and synaptic activity in hippocampal cell cultures. NeuroReport 8:3791–3794.

Bibel M, Barde YA (2000) Neurotrophins: key regulators of cell fate and cell shape in the vertebrate nervous system. Genes Dev 14:2920–2935.

Bolton MM, Pittman AJ, Lo DC (2000) Brain-derived neurotrophic factor differentially regulates excitatory and inhibitory synaptic transmission in hippocampal cultures. J Neurosci 20:3221–3232.

Causing CG, Gloster A, Aloyz R, Bamji SX, Chang E, Fawcett J, Kuchel G, Miller FD (1997) Synaptic innervation density is regulated by neuron-derived BDNF. Neuron 18:257–267.

Cellerino A, Maffei L, Domenici L (1996) The distribution of brain-derived neurotrophic factor and its receptor trkB in parvalbumin-containing neurons of the rat visual cortex. Eur J Neurosci 8:1190–1197.

Drake CT, Milner TA, Patterson SL (1999) Ultrastructural localization of full-length trkB immunoreactivity in rat hipppcampus suggests multiple roles in modulating activity-dependent synaptic plasticity. J Neurosci 19:8009–8026.

Erlander MG, Tobin AJ (1991) The structural and functional heterogeneity of glutamic acid decarboxylase: a review. Neurochem Res 16:215–226.

Ernfors P, Wetmore C, Olson L, Persson H (1990) Identification of cells in rat brain and peripheral tissues expressing mRNA for members of the nerve growth factor family. Neuron 5:511–526.

Fawcett JP, Alonso-Vanegas MA, Morris SJ, Miller FD, Sadikot AF, Murphy RA (2000) Evidence that brain-derived neurotrophic factor from presynaptic nerve terminals regulates the phenotype of calbindin-containing neurons in the lateral septum. J Neurosci 20:274–282.

Frerking M, Malenka RC, Nicoll RA (1998) Brain-derived neurotrophic factor (BDNF) modulates inhibitory, but not excitatory, transmission in the CA1 region of the hippocampus. J Neurophysiol 80:3383–3386.

Friedman WJ, Black IB, Kaplan DR (1998) Distribution of the neurotrophins brain-derived neurotrophic factor, neurotrophin-3, and neurotrophin-4/5 in the postnatal rat brain: an immnunocytochemical study. Neuroscience 84:101–114.

Fujikawa N, Tominaga-Yoshino K, Okabe M, Ogura A (2000) Depolarization-dependent survival of cultured mouse cerebellar granule neurons is strain-restrained. Eur J Neurosci 12:1838–1842.

Gartner A, Staiger V (2002) Neurotrophin secretion from hippocampal neurons evoked by long-term potentiation-inducing electrical stimulation patterns. Proc Natl Acad Sci USA 99:6386–6391.

Goodman LJ, Valverde J, Lim F, Geschwind MD, Federoff HJ, Geller AI, Hefti F (1996) Regulated release and polarized localization of brain-derived neurotrophic factor in hippocampal neurons. Mol Cell Neurosci 7:222–238.

Gorba T, Wahle P (1999) Expression of TrkB and TrkC but not BDNF mRNA in neurochemically identified interneurons in rat visual cortex *in vivo* and in organotypic cultures. Eur J Neurosci 11:1179–1190.

Hanover JL, Huang ZJ, Tonegawa S, Stryker MP (1999) Brain-derived neurotrophic factor overexpression induces precocious critical period in mouse visual cortex. J Neurosci 19:RC40.

Hartmann M, Heumann R, Lessmann V (2001) Postsynaptic release of brain-derived neurotrophic factor induced by high frequency synaptic stimulation. EMBO J 20:5887–5897.

Hensch TK, Fagiolini M, Mataga N, Stryker MP, Baekkeskov S, Kash SF (1998) Local GABA circuit control of experience-dependent plasticity in developing visual cortex. Science 282:1504–1508.

Horch HE, Kruttgen A, Portbury SD, Katz LC (1999) Destablization of cortical dendrites and spines by BDNF. Neuron 23:353–364.

Huang ZJ, Kirkwood A, Pizzorusso T, Porciatti V, Morales B, Bear MF, Maffei L, Tonegawa S (1999) BDNF regulates the maturation of inhibition and the critical period of plasticity in mouse visual cortex. Cell 98:739–755.

Ip NY, Li Y, Yancopoulos GD, Lindsay R (1993) Cultured hippocampal neurons show responses to BDNF, NT-3, and NT-4, but not NGF. J Neurosci 13:3394–3405.

Itami C, Mizuno K, Kohno T, Nakamura S (2000) Brain-derived neurotrophic factor requirement for activity-dependent maturation of glutamatergic synapse in developing mouse somatosensory cortex. Brain Res 857:141–150.

Ivkovic S, Ehrlich ME (1999) Expression of the striatal DARPP-32/ARPP-21 phenotype in GABAergic neurons requires neurotrophins *in vivo* and *in vitro*. J Neurosci 19:5409–5419.

Iwasato T, Datwani A, Wolf AM, Nishiyama H, Taguchi Y, Tonegawa S, Knopfel T, Erzurumlu RS, Itohara S (2000) Cortex-restricted disruption of NMDAR1 impairs neuronal patterns in the barrel cortex. Nature 406:726–731.

Johnson RR, Burkhalter A (1996) Microcircuitry of forward and feedback connections within rat visual cortex. J Comp Neurol 368:383–398.

Kaneko T, Mizuno N (1988) Immunohistochemical study of glutaminase-containing neurons in the cerebral cortex and thalamus of the rat. J Comp Neurol 267:590–602.

Katoh-Semba R, Takeuchi IK, Semba R, Kato K (1997) Distribution of brain-derived neurotrophic factor in rats and its changes with development in the brain. J Neurochem 69:34–42.

Katoh-Semba R, Takeuchi IK, Inaguma Y, Ichisaka S, Hata Y, Tsumoto T, Iwai M, Mikoshiba K, Kato K (2001) Induction of brain-derived neurotrophic factor by convulsive drugs in the rat brain: involvement of region-specific voltage-dependent calcium channels. J Neurochem 77:71–83.

Kisvarday ZF (1992) GABAergic networks of basket cells in the visual cortex. Prog Brain Res 90:385–405.

Kohara K, Kitamura A, Morishima M, Tsumoto T (2001) Activity-dependent transfer of brain-derived neurotrophic factor to postsynaptic neurons. Science 291:2419–2423.

Kojima M, Takei N, Numakawa T, Ishikawa Y, Suzuki S, Matsumoto T, Katoh-Semba R, Nawa H, Hatanaka H (2001) Biological characterization and optical imaging of BDNF-GFP suggest an activity-dependent local release of BDNF in neurites of cultured hippocampal neurons. J Neurosci Res 64:1–10.

Kokaia ZJ, Bengson M, Matsis M, Kokaia M, Persson H (1993) Coexpression of neurotrophins and their receptors in neurons of the central nervous system. Proc Natl Acad Sci USA 90:6711–6715.

Lever IJ, Bradbury EJ, Cunningham JR, Adelson DW, Jones MG, McMahon SB, Marvizon JC, Malcangio M (2001) Brain-derived neurotrophic factor is released in the dorsal horn by distinctive patterns of afferent fiber stimulation. J Neurosci 21:4469–4477.

Marty S, Berninger B, Carroll P, Thoenen H (1996) GABAergic stimulation regulates the phenotype of hippocampal interneurons through the regulation of brain-derived neurotrophic factor. Neuron 16:565–570.

Marty S, Berzaghi MD, Berninger B (1997) Neurotrophins and activity-dependent plasticity of cortical interneurons. Trends Neurosci 20:198–202.

Marty S, Wehrle R, Sotelo C (2000) Neuronal activity and brain-derived neurotrophic factor regulate the density of inhibitory synapses in organotypic slice cultures of postnatal hippocampus. J Neurosci 20:8087–8095.

McAllister AK, Lo DC, Katz LC (1995) Neurotrophins regulate dendritic growth in developing visual cortex. Neuron 15:791–803.

McAllister AK, Katz LC, Lo DC (1996) Neurotrophin regulation of cortical dendritic growth requires activity. Neuron 17:1057–1064.

McAllister AK, Katz LC, Lo DC (1997) Opposing roles for endogenous BDNF and NT-3 in regulating cortical dendritic growth. Neuron 18:767–778.

McAllister AK, Katz LC, Lo DC (1999) Neurotrophins and synaptic plasticity. Annu Rev Neurosci 22:295–318.

Minichiello L, Korte M, Wolfe D, Kuhn R, Unsicker K, Cestari V, Rossi-Arnaud C, Lipp HP, Bonhoeffer T, Klein R (1999) Essential role for TrkB receptors in hippocampus-mediated learning. Neuron 24:401–414.

Miranda RJ, Sorabji F, Torrand-Allerand D (1993) Neuronal colocaliztion of mRNAs for neurotrophins and their receptors in the developing central nervous system suggests a potential for autocrine interactions. Proc Natl Acad Sci USA 90:6439–6443.

Mizuno K, Carnahan Y, Nawa H (1994) Brain-derived neurotrophic factor promotes differentiation of striatal GABAergic neurons. Dev Biol 165:243–256.

Nawa H, Bessho Y, Carnahan Y, Nakanishi S, Mizuno K (1993) Regulation of neuropeptide expression in cultured cerebral cortical neurons by brain-derived neurotrophic factor. J Neurochem 60:772–775.

Nawa H, Carnahan J, Gall C (1995) BDNF protein measured by a novel enzyme immunoassay in normal brain and after seizure: partial disagreement with mRNA levels. Eur J Neurosci 7:1527–1535.

Okabe M, Ikawa M, Kominami K, Nakanishi T, Nishimune Y (1997) "Green mice" as a source of ubiquitous green cells. FEBS Lett 407:313–319.

Poo MM (2001) Neurotrophins as synaptic modulators. Nat Rev Neurosci 2:24–32.

Rocamora N, Welker E, Pascual M, Soriano E (1996) Upregulation of BDNF mRNA in the barrel cortex of adult mice after sensory stimulation. J Neurosci 16:4411–4419.

Rutherford LC, DeVan A, Lauer HM, Turrigiano GG (1997) Brain-derived neurotrophic factor mediates the activity-dependent regulation of inhibition in neocortical cultures. J Neurosci 17:4527–4535.

Rutherford LC, Nelson SB, Turrigiano GG (1998) BDNF has opposite effects on the quantal amplitude of pyramidal neuron and interneuron excitatory synapses. Neuron 21:521–530.

Schinder AF, Berninger M, Poo MM (2000) Postsynaptic target specificity of neurotrophin-induced presynaptic potentiation. Neuron 25:151–163.

Schmidt-Kastner R, Wetmore C, Olson L (1996) Comparative study of brain-derived neurotrophic factor messenger RNA and protein at the cellular level suggests multiple roles in hippocampus, striatum and cortex. Neuroscience 74:161–183.

Schwartz PM, Borghesani PR, Levy RL, Pomeroy SL, Segal RA (1997) Abnormal cerebellar development and foliation in BDNF−/− mice reveals a role for neurotrophins in CNS patterning. Neuron 19:269–281.

Takei N, Kawamura M, Hara K, Yonezawa K, Nawa H (2001) Brain-derived neurotrophic factor enhances neuronal translation by activating multiple initiation processes. J Biol Chem 276:42818–42825.

Tanaka T, Saito H, Matsuki N (1997) Inhibition of $GABA_A$ synaptic responses by brain-derived neurotrophic factor (BDNF) in rat hippocampus. J Neurosci 17:2959–2966.

Thoenen H (1995) Neurotrophins and neuronal plasticity. Science 270:593–598.

Tsien JZ, Chen DF, Gerber D, Tom C, Mercer EH, Anderson DJ, Mayford M, Kandel ER, Tonegawa S (1996) Subregion- and cell type-restricted gene knockout in mouse brain. Cell 87:1317–1326.

Vicario-Abejon C, Collin C, McKay RDG, Segal M (1998) Neurotrophins induce formation of functional excitatory and inhibitory synapses between cultured hippocampal neurons. J Neurosci 18:7256–7271.

Watson FL, Heerssen HM, Moheban DB, Lin MZ, Sauvageot CM, Bhattacharyya A, Pomeroy SL, Segal RA (1999) Rapid nuclear responses to target-derived neurotrophins require retrograde transport of ligand-receptor complex. J Neurosci 19:7889–7900.

Xu B, Gottschalk W, Chow A, Wilson RI, Schnell E, Zang K, Wang D, Nicoll RA, Lu B, Reichardt LF (2000a) The role of brain-derived neurotrophic factor receptors in the mature hippocampus: Modulation of long-term potentiation through a presynaptic mechanism involving TrkB. J Neurosci 20:6888–6897.

Xu B, Zang K, Ruff NL, Zhang A, McConnell SK, Stryker MP, Reichardt LF (2000b) Cortical degeneration in the absence of neurotrophin signaling: Dendritic retraction and neuronal loss after removal of the receptor TrkB. Neuron 26:233–245.

Yamada MK, Nakanishi K, Ohba S, Nakamura T, Ikegaya Y, Nishiyama N, Matsuki N (2002) Brain-derived neurotrophic factor promotes the maturation of GABAergic mechanisms in cultured hippocampal neurons. J Neurosci 22:7580–7585.

Yan Q, Rosenfeld RD, Matheson CR, Hawkins N, Lopez OT, Bennett L, Welcher AA (1997) Expression of brain-derived neurotrophic factor protein in the adult rat central nervous system. Neuroscience 78:431–448.

Abbreviated incubation times for human prions in mice expressing a chimeric mouse–human prion protein transgene

Carsten Korth[a,b], Kiyotoshi Kaneko[a,c], Darlene Groth[a], Norbert Heye[a,d], Glenn Telling[a,e], James Mastrianni[a,f], Piero Parchi[g,h], Pierluigi Gambetti[g], Robert Will[i], James Ironside[j], Cornelia Heinrich[a], Patrick Tremblay[a,k,l], Stephen J. DeArmond[a,m], and Stanley B. Prusiner[a,k,n,o]

[a]Institute for Neurodegenerative Diseases and Departments of [k]Neurology, [m]Pathology, and [n]Biochemistry and Biophysics, University of California, San Francisco, CA 94143; [g]Division of Neuropathology, Case Western Reserve University, Cleveland, OH 44106; [i]National CJD Surveillance Unit, Western General Hospital, Edinburgh EX4 2HU, United Kingdom; and [j]Neuropathology Laboratory, University of Edinburgh, Edinburgh EH8 9LJ, United Kingdom

Contributed by Stanley B. Prusiner, December 30, 2002

Transgenic (Tg) mouse lines that express chimeric mouse–human prion protein (PrP), designated MHu2M, are susceptible to prions from patients with sporadic Creutzfeldt–Jakob disease (sCJD). With the aim of decreasing the incubation time to fewer than 200 days, we constructed transgenes in which one or more of the nine human residues in MHu2M were changed to mouse. The construct with murine residues at positions 165 and 167 was expressed in Tg(MHu2M,M165V,E167Q) mice and resulted in shortening the incubation time to ≈110 days for prions from sCJD patients. The construct with a murine residue at position 96 resulted in lengthening the incubation time to more than 280 days for sCJD prions. When murine residues 96, 165, and 167 were expressed, the abbreviated incubation times for sCJD prions were abolished. Variant CJD prions showed prolonged incubation times between 300 and 700 days in Tg(MHu2M) mice on first passage and incubation times of ≈350 days in Tg(MHu2M,M165V,E167Q) mice. On second and third passages of variant CJD prions in Tg(MHu2M) mice, multiple strains of prions were detected based on incubation times and the sizes of the protease-resistant, deglycosylated PrP^{Sc} fragments. Our discovery of a previously undescribed chimeric transgene with abbreviated incubation times for sCJD prions should facilitate studies on the prion species barrier and human prion diversity.

Human prion diseases include Creutzfeldt–Jakob disease (CJD), kuru, and fatal insomnia (FI; ref. 1). Sporadic (s) CJD accounts for ≈85% of all cases of human prion disease, familial (f) CJD for 10–15%, and infection from exogenous prions for <1% (2). Prions consist solely of a pathogenic prion protein, denoted PrP^{Sc}, that is derived from the cellular isoform PrP^{C} (1, 3). Replication of prions occurs when PrP^{Sc} stimulates conversion of PrP^{C} into nacent PrP^{Sc}. It seems likely that a cofactor participates in the formation of PrP^{Sc} (4, 5); one such cofactor, provisionally designated protein X, has been invoked to explain dominant-negative inhibition of prion replication. Using scrapie-infected neuroblastoma (ScN2a) cells, the putative binding site of protein X on PrP was mapped (6).

Transmission of human prions to wild-type (wt) rodents was difficult because of the "species barrier" (7) that appears to be modulated by (*i*) the degree of homology between PrP sequences (8–10), (*ii*) cofactors such as protein X, and (*iii*) the prion strain. Although incubation times of ≈200 days in transgenic (Tg) mice greatly accelerated studies of human prion disease, the prolonged duration has hampered many studies (4, 11, 12).

Within a single species, strains of prions stably transmit a particular disease phenotype, characterized by the length of the incubation time, clinical signs as well as patterns of PrP^{Sc} deposition and neuropathological lesions (13, 14). A growing body of evidence argues that strain-specific properties of prions are enciphered in the conformation of PrP^{Sc} (15–19). Strains of sCJD prions have been classified according to the amino acid at position 129 [methionine (M) or valine (V)] and with respect to the electrophoretic gel mobility (21 or 19 kDa, as type 1 or type 2, respectively) of the deglycosylated, protease-resistant (r) PrP^{Sc} fragment (20). Employing this analysis, 70% of sCJD cases are either MM1 or MV1, and 24% are either VV2 or MV2. In addition to the sCJD strains, a new strain of CJD prions, termed variant CJD (vCJD), has been found (21). This strain is thought to have originated in cattle with bovine spongiform encephalopathy (BSE) and was transmitted to humans through ingestion of BSE-tainted beef products (18, 22, 23).

To define the molecular basis of the species barrier and to produce mice with shorter incubation times, we mutagenized the chimeric mouse–human (MHu2M) transgene. Substitution of mouse residues at positions 165 and 167 in the Hu2 insert reduced the incubation time by nearly 50% for sCJD and fCJD prions. Whether these substitutions shorten the incubation time by optimizing the interaction of the transgene product with protein X is unknown. Investigations of vCJD prions serially passaged in Tg(MHu2M) mice demonstrated the existence of multiple strains.

Methods

Production of Tg Mice. In MHu2M, the N and C termini are from mouse PrP and the central "Hu2" insert corresponding to residues 96–167, is from human PrP (11). Tg mice were produced as described (8, 24), except that purified cos.SHa.Tet fragments containing the respective constructs were microinjected into the pronuclei of fertilized oocytes from FVB/$Prnp^{0/0}$ mice (25). Constructs were cloned by using mismatch primer mutagenesis (8). Genomic DNA isolated from weanling animals was screened for the incorporation of the transgene by using probes hybridizing to the 3′ UTR of the cos.SHa.Tet vector (1). Tg(HuPrP,M129)440/$Prnp^{0/0}$ mice express $HuPrP^{C}$ with M at 129 and at 2× the level found in human brain. Tg(HuPrP,V129)152/$Prnp^{0/0}$ mice express $HuPrP^{C}$ with V at 129 and at 4–8× the level found in the human brain. In Tg(MHu2M)5378/$Prnp^{0/0}$ mice, PrP^{C} is expressed at 2× the level found in Syrian hamster brain.

Abbreviations: PrP, prion protein; PrP^{C}, normal cellular isoform; PrP^{Sc}, disease-associated isoform; Tg, transgenic; CJD, Creutzfeldt–Jakob disease; vCJD, variant CJD; sCJD, sporadic CJD.

[b]Present address: Institut für Neuropathologie, Heinrich-Heine Universität Düsseldorf, Düsseldorf 40001, Germany.

[c]Present address: National Center of Neurology and Psychiatry, and Core Research for Evolutional Science and Technology, Kodaira, Tokyo 187-8502, Japan.

[d]Present address: Klinik für Neurochirurgie der Universität zu Köln, Cologne 50931, Germany.

[e]Present address: Department of Microbiology and Immunology, University of Kentucky, Lexington, KY 40536.

[f]Present address: Department of Neurology, University of Chicago, Chicago, IL 60637.

[h]Present address: Department of Neurological Sciences, University of Bologna, Bologna 40123, Italy.

[l]Present address: Neurochem, Inc., Ville St. Laurent, QC, Canada H4S 2A1.

[o]To whom correspondence should be addressed. E-mail: stanley@itsa.ucsf.edu.

www.pnas.org/cgi/doi/10.1073/pnas.2627989100

Table 1. Transmission of human prions to transgenic mice expressing MHu2M(M165V,E167Q), MHu2M, HuPrP(M129), or HuPrP(V129)

Inoculum	Incubation period in days ± SEM (n/n_0*)			
	MHu2M(M165V,E167Q) Tg22372	MHu2M Tg5378	HuPrP(M129) Tg440	HuPrP(V129) Tg152
MM1†				
RG	106 ± 2 (13/13)‡	191 ± 3 (10/10)	165 ± 4 (7/7)	263 ± 2 (6/6)
EC	114 ± 2 (7/7)§		157 ± 3 (7/7)	254 ± 6 (9/9)
HS	111 ± 2 (7/7)§	196 ± 4 (8/8)	163 ± 2 (9/9)	
Ho		205 ± 7 (6/6)	155 ± 3 (8/8)	
DG	106 ± 2 (7/7)§			
AM	112 ± 2 (8/8)¶			
MM2				
A88-418		>680 (0/10)	232 ± 5 (3/3)	368 ± 19 (9/9)
094-3		>650 (0/7)	>580 (0/8)	556 ± 63 (5/5)
sFI-St‖	303 ± 20 (4/6)	221 ± 6 (4/4)	699 ± 30 (2/5)	
vCJD-RU96/45**	335 ± 23 (7/7)	647 ± 35 (2/7)		
vCJD-RU96/02**	380 ± 10 (6/6)	563 ± 201 (4/7)		
MV1				
WP	124 ± 3 (7/7)§	214 ± 3 (8/8)		
Ghi		215 ± 4 (5/5)		
Ro			176 ± 2 (9/9)	
MV2				
093-25		>640 (0/10)	350 ± 38 (3/6)	209 ± 3 (7/7)
A94-311		>640 (0/10)	419 ± 13 (9/9)	206 ± 3 (6/6)
096-48		>640 (0/10)	307 ± 27 (7/9)	231 ± 4 (5/5)
AMB	>450 (0/10)			
VV2				
RP	>450 (1/10)	531 ± 46 (3/14)	248 ± 12 (3/7)	223 ± 7 (7/7)
A90-332		>500 (0/8)	448 ± 34 (3/7)	195 ± 3 (8/8)
094-87		433 (1/10)	378 ± 7 (3/7)	198 ± 5 (9/9)
GF	>450 (2/10)			

*n, number of diseased animals; n_0, number of inoculated animals.
†Strain typing as described in ref. 20.
‡§¶Number of animals that died by a cause other than prion disease: 5 (‡), 3 (§), 2 (¶).
‖Inoculum from patient with sporadic FI.
**Inocula from patients with vCJD.

Human Brain Inocula. Patient diagnoses were confirmed by histopathology, immunohistochemistry, and detection of human PrP^{Sc} by Western blotting (20, 26). Patients were genotyped (4) by DNA sequencing of the entire ORF after extracting genomic DNA either from leukocytes collected during life or from frozen brain after death.

Preparation of Brain Homogenates and Bioassays. Ten percent homogenates of sCJD human brains or Tg mouse brains were prepared as described (4). Bioassays were performed as described (27). After onset of disease symptoms, mice were killed and their brains were immediately frozen or fixed in formalin. For neuropathology, brains were immersion-fixed in a 10% buffered formalin solution and embedded in paraffin. Immunohistochemistry for PrP on formalin-fixed, paraffin-embedded tissue sections was performed using the hydrolytic autoclaving technique (28). Histoblot analysis was performed as described (29).

Results

Tg Mice Expressing MHu2M PrP. sCJD transmits to Tg(MHu2M)5378/$Prnp^{0/0}$ mice with an incubation time of ≈200 days (11) (Fig. 4*a*, which is published as supporting information on the PNAS web site, www.pnas.org); these mice are subsequently referred to as Tg5378 mice. Because an inverse relationship was found previously between the level of PrP transgene expression and the length of the incubation time (30), six Tg lines expressing higher levels of MHu2M were constructed and inoculated with sCJD(MM1) prions. The lines with 8× expression levels had incubation periods of 160 ± 3 days (n/n_0 = 10/10), 177 ± 4 days (n/n_0 = 10/10), and 209 ± 4 days (n/n_0 = 10/10). The lines with 32× expression levels showed longer incubation periods of 233 ± 4 days (n/n_0 = 10/10), 236 ± 5 days (n/n_0 = 11/11), and 239 ± 4 days (n/n_0 = 11/11). Thus, raising the level of MHu2M expression did not reduce the incubation time.

Mutagenesis of the MHu2M Transgene. Because of the limitations posed by the production of Tg mouse lines, we decided to change some of nine human residues in the Hu2 insert of MHu2M to those encoded by MoPrP (Fig. 5, which is published as supporting information on the PNAS web site). Five single substitutions were made: three at the N-terminal positions S96N, M108L, and M111V, and two at the C-terminal positions M165V and E167Q. We also combined some of the five mutated residues to create double and triple substitutions.

Abbreviated Incubation Times in Tg(MHu2M,M165V,E167Q) Mice. Because none of the single substitutions except possibly residue M165V seemed promising, we constructed Tg mice expressing the doubly substituted MHu2M(M165V,E167Q) transgene. The first line, Tg(MHu2M,M165V,E167Q)22372/$Prnp^{0/0}$, subsequently referred to as Tg22372 mice, express chimeric PrP at a level of 1–2×. Tg22372 mice were inoculated with brain homogenates from 10 different sCJD cases (Table 1, see a representative case depicted in Fig. 4*d*), one case with fCJD(E200K) (Fig. 4*e*), one case with

familial FI [FFI(MV2,D178N)] (Fig. 4*f*), and one case of sporadic FI (sFI; ref. 31). Strikingly, the mean incubation times after inoculation with sCJD(MM1) prions were reduced by nearly 50% compared with those in Tg5378 mice; they ranged from 106 to 114 days (Table 1). No sCJD(VV2) cases have transmitted disease at >450 days after inoculation. fCJD(E200K) prions transmitted disease in 109 days on first passage and in 100 days on second passage, similar to sCJD(MM1) prions. FFI and sFI prions transmitted inefficiently to Tg22372 mice; the animals exhibited incubation times of 263 ± 15 days (n/n_0 = 5/6) and 303 ± 20 days, respectively. On second passage of FFI prions in Tg22372 mice, the incubation time was reduced from 263 days to 97 days (Fig. 4*f*). Uninoculated Tg22372 mice remained healthy for more than 620 days.

These strain-specific patterns of incubation times from different inocula are similar to those found with Tg5378 mice. When brain homogenates from patients with fCJD(E200K) were inoculated into Tg5378 mice, the incubation time was 170 ± 2 days (n/n_0 = 10/10) and did not change on second passage (Fig. 1*b*). Inoculation of Tg5378 mice with brain homogenates from three patients with FFI(MV2,D178N) produced incubation times of 247 ± 6 days (n/n_0 = 7/7), 206 ± 7 days (7/7), and 193 ± 5 days (9/9) on first passage, which shortened on second passage to 123 ± 3 days (7/7), 132 ± 5 days (9/9), and 136 ± 1 days (6/6), respectively (see a representative case depicted in Fig. 4*c*). Interestingly, the shortening of incubation times on second passage demonstrates a similar transmission barrier for FFI prions in both Tg5378 and Tg22372 mice (compare Fig. 4 *c* and *f*).

Additional Tg(MHu2M,M165V,E167Q)*Prnp*$^{0/0}$ mice were derived from two other founders. The chimeric MHu2M (M165V,E167Q) was expressed at 4–8× as measured by mRNA expression. Many of these Tg(MHu2M,M165V,E167Q)*Prnp*$^{0/0}$ mice developed ataxia between 120 and 150 days of age and thus, neither line was inoculated. Mice killed at 200 days of age exhibited widespread astrocytic gliosis in the caudate and putamen, but no neuronal loss was observed. Faint, minimal punctate deposits of mutant PrP^{Sc} detected by immunostaining with the chimeric human–mouse recombinant Fab D18 and the 3F4 mAb were found only in the caudate and putamen (data not shown). The hippocampus and cerebellum showed no pathologic changes.

Biochemical Characteristics of Chimeric Mouse–Human Prions. For sCJD and fCJD(E200K) prions, the molecular size of the deglycosylated $rPrP^{Sc}$ fragment was 21 kDa (type 1) (Fig. 1*a*, lanes 1 and 4). The same-sized PrP^{Sc} fragments were found in the brains of Tg5378 mice after first and second passages of either sCJD or fCJD(E200K) prions (Fig. 1*a*, lanes 2, 3, 5, and 6). For FFI, the molecular size of deglycosylated $rPrP^{Sc}$ was 19 kDa (type 2) (Fig. 1*a*, lane 7). Although the incubation times for FFI prions decreased nearly 50% on second passage in Tg5378 mice (Fig. 4*c*), the molecular size of the deglycosylated, $rPrP^{Sc}$ fragment remained 19 kDa (Fig. 1*a*, lanes 8 and 9). These findings clearly dissociate the size of the deglycosylated, $rPrP^{Sc}$ fragment from the incubation time.

Western blots of brain homogenates from sCJD patients and from corresponding inoculated Tg22372 mice demonstrated $rPrP^{Sc}$ (Fig. 1*b*). Three different cases of sCJD (Fig. 1*b*, lanes 1–3, 8–10, and 15–17) were passaged into Tg22372 mice and produced MHu2M(M165V,E167Q) prions (Fig. 1*b*, lanes 4–6 and 11–13). Uninoculated mice did not produce MHu2M(M165V,E167Q) prions (Fig. 1*b*, lanes 7 and 14). Brain homogenates from sCJD(MM1) (RG) inoculated into Tg22372 mice (Fig. 1*c*, lanes 2, 6, and 10) were repassaged into the same line (Fig. 1*c*, lanes 3, 7, and 11), and into Tg5378 mice (Fig. 1*c*, lanes 4, 8, and 12). On passage into Tg22372 mice, slight changes of the glycosylation pattern were seen (compare Fig. 1*c*, lane 5 with lanes 6 and 7), but there were no changes in deglycosylated $rPrP^{Sc}$ (Fig. 1*c*, lanes 9–12).

MHu2M(M165V,E167Q) prions from sCJD(MM1) (RG) inoc-

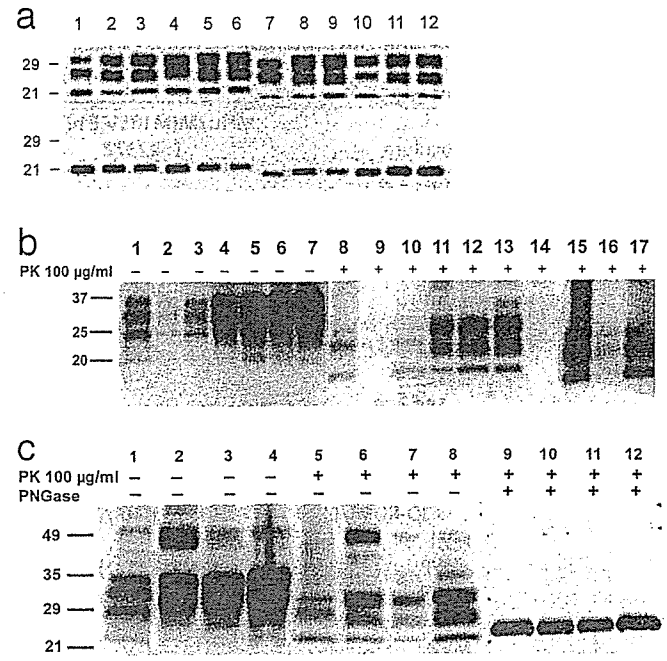

Fig. 1. Western blots of brain homogenates from inocula and inoculated Tg5378 and Tg22372 mice. (*a*) Immunoblots of $rPrP^{Sc}$ (*Upper*) and deglycosylated $rPrP^{Sc}$ (*Lower*) from brain homogenates, inoculated first and second passages, respectively, of sCJD(MM1) (lanes 1–3), fCJD(E200K) (lanes 4–6), FFI (lanes 7–9), and vCJD (lanes 10–12) into Tg5378 mice. In the first lane of each triplet (lanes 1, 4, 7, and 10), PrP^{Sc} in homogenates of the diseased human brains is shown; in the second lane of each triplet (lanes 2, 5, 8, and 11), PrP^{Sc} in brain homogenates of Tg5378 mice inoculated with diseased human brains is shown; and in the third lane of each triplet (lanes 3, 6, 9, and 12), PrP^{Sc} in brain homogenates from Tg5378 mice inoculated with diseased Tg5378 brain homogenates (from first passage of human prions) is shown. (*b*) Undigested brain homogenates from sCJD (RG) (lane 1); sCJD (EC) (lane 2); sCJD (WP) (lane 3), and Tg22372 mice inoculated with sCJD (RG) (lane 4); sCJD (EC) (lane 5); and sCJD (WP) (lane 6). Lane 7 shows an uninoculated Tg22372 mouse. Lanes 8–14 show the same brain homogenates as lanes 1–7, respectively, but brain homogenates were digested with proteinase K. Lanes 15–17 are the same as lanes 8–10, respectively, except the film was exposed longer to detect the weak band of PrP^{Sc} in lane 16. The blot clearly shows the overexpression of PrP in the brains of transgenic mice relative to human brains (compare lane 7 with lanes 1–3). (*c*) Brain homogenates from sCJD(MM1) (RG) (lanes 1, 5, and 9) and from Tg22372 mice inoculated with sCJD (RG) on first passage (lanes 2, 6, and 10) and second passage (lanes 3, 7, and 11). Brain homogenate from the second passage of sCJD (RG) into Tg5378 mice are shown in lanes 4, 8, and 12. Lanes 1–4 show undigested brain homogenates, lanes 5–8 show brain homogenates after 100 μg/ml PK digestion, and lanes 9–12 show brain homogenates after both PK digestion and PNGase F digestion. The glycoform pattern of PrP^{Sc} changes from the original sCJD (RG) pattern (lane 5) to the first passage (lane 6), remains the same on second passage (lane 7) but changes when passaged into Tg5378 mice (lane 8). The gel mobility of deglycosylated $rPrP^{Sc}$ does not change (compare lane 9 to lanes 10–12).

ula produced incubation times of 95 ± 2 days when passaged into Tg22372 mice (Fig. 4*d*), and of 166 ± 3 days when passaged into Tg5378 mice. MHu2M(M165V,E167Q) prions could not be passaged into Tg(MoPrP)4053/FVB mice overexpressing wt mouse PrP, indicating that chimeric MHu2M(M165V,E167Q) prions are unlikely to cross this transmission barrier.

PrP^{Sc} Deposition in Tg22372 Mice. Tg22372 mice were inoculated with sCJD(MM1), fCJD, FFI, sFI, or vCJD prions. Histoblotting of brain sections showed that each of these inocula produced a different pattern of PrP^{Sc} deposition. Brains from Tg22372 mice infected with prions from six cases of sCJD(MM1) showed similar patterns of PrP^{Sc} deposition (Fig. 2 *a* and *b*; and Fig. 6, which is published as supporting information on the PNAS web site). PrP^{Sc}

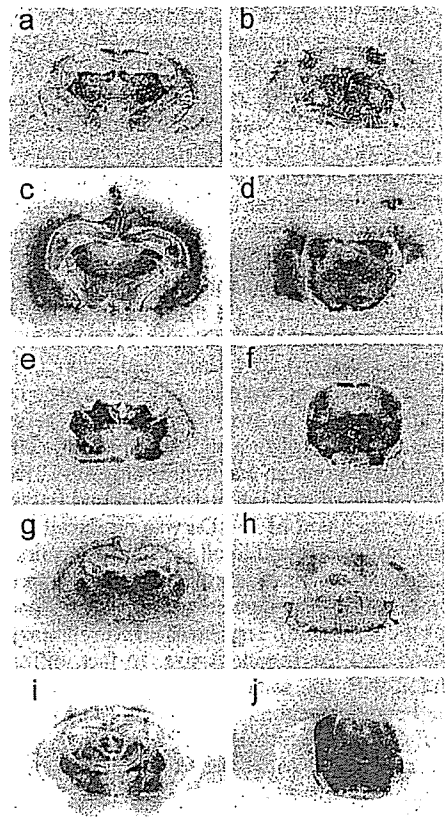

Fig. 2. PrP^{Sc} deposition shown by histoblotting in Tg22372 mice inoculated with different forms of CJD and FI. Coronal sections through the thalamic-hippocampal area (*a*, *c*, *e*, *g*, and *i*) or midbrain-pons area (*b*, *d*, *f*, *h*, and *j*) are depicted. Histoblots showing PrP^{Sc} deposition patterns after inoculation with sCJD(MM1)(RG) (*a* and *b*), fCJD(E200K) (*c* and *d*), FFI (*e* and *f*), sFI (*g* and *h*), and vCJD (*i* and *j*).

was deposited in the habenula, thalamus, colliculi nucleus, and midbrain tegmentum as well as the inner half of the cerebral cortex (Fig. 2 *a* and *b*). Some, but not all, white matter tracts were also immunopositive, including the corpus callosum (Fig. 2*a*) and the habenulopeduncular tract of the midbrain. The internal capsule and cerebral peduncles were negative. In contrast to sCJD prions, fCJD(E200K) prions produced widespread accumulation of PrP^{Sc}, in the cerebral cortex and hippocampus as well as much of the thalamus and hypothalamus, and most nuclei of the brainstem (Fig. 2 *c* and *d*). FFI prions produced the most intense immunostaining of the thalamus, lateral hypothalamus and brainstem (Fig. 2 *e* and *f*). sFI prions also produced intense PrP^{Sc} immunostaining of the thalamus (Fig. 2*g*), but little staining was found in the brainstem (Fig. 2*h*). In Tg22372 mice inoculated with vCJD prions, intense immunostaining in the tegmentum of the brainstem was found with less intensity in the thalamus and hypothalamus, but no PrP^{Sc} was seen in the cerebral cortex (Fig. 2 *i* and *j*). Punctate PrP^{Sc} deposits that correspond to PrP amyloid were distributed over the surface of the hippocampus (Fig. 2*i*). PrP immunopositive amyloid plaques (Fig. 6 *l* and *p*), particularly in the subcallosal region overlying the hippocampus, were associated with intense reactive astrocytic gliosis (Fig. 6*n*).

Like the similar patterns of PrP^{Sc} deposition, the intensity and distribution of vacuolation as well as reactive astrocytic gliosis in Tg22372 mice were indistinguishable for the six different cases of sCJD(MM1) (Figs. 7 and 8, which are published as supporting information on the PNAS web site). Moreover, the brains of Tg22372 and Tg5378 mice inoculated with the same CJD strains were virtually indistinguishable on pathologic examination. For each sCJD inoculum, the vacuolation scores (percentage of an area occupied by vacuoles) for the inner half of the cerebral cortex were 2× greater than those for the outer half. The degree of vacuolation in the thalamus, caudate nucleus and brainstem was similar (Fig. 7). No vacuolation was found in the cerebellar cortex with any of the sCJD inocula. Immunohistochemistry for PrP^{Sc} by hydrolytic autoclaving showed deposits ranging from finely granular (synaptic-like) to coarse and primitive (plaque-like); however, differences among inocula did not seem to be significant (Fig. 7). No differences between first and second passage of sCJD (RG) in Tg22372 mice were found on neuropathological examination (Fig. 7).

The combined findings for six sCJD(MM1) cases suggest that the prions in each case might be similar or indistinguishable strains. However, additional studies are required to test this conjecture, including end-point titrations, which yield dose-response curves. The slopes of these curves have been used to distinguish different prion strains (32).

Single and Triple Substitutions in MHu2M Transgenes. Tg mouse lines were generated expressing MHu2M(M165V) and MHu2M(E167Q). Tg(MHu2M,E167Q)18990/$Prnp^{0/0}$ mice overexpressing MHu2M(E167Q) at a level of ≈8× developed spontaneous neurodegenerative disease with frequent symptoms of dysmetria and proprioceptive deficits and less frequently, hindlimb paresis ending in death at ≈300 days of age. Neuropathological examination showed no vacuolation or obvious nerve cell loss; however, generalized reactive astrocytic gliosis accentuated in the caudate nucleus, brainstem, and cortex was found (Fig. 9, which is published as supporting information on the PNAS web site). PrP staining showed unusual punctate, perinuclear deposits in the pyramidal cell layer and in the hippocampus. No $rPrP^{Sc}$ was detected in brain homogenates (data not shown) and no infectivity was found by inoculating Tg5378 mice, which have remained well for >524 days.

Tg(MHu2M,M165V)17030/$Prnp^{0/0}$ mice inoculated with sCJD(MM1) (RG) prions had shortened incubation times of 105 ± 2 days (n/n_0 = 10/10) on first passage and 92 ± 2 days (n/n_0 = 10/10) on second passage. However, a second line, Tg(MHu2M,M165V)17000/$Prnp^{0/0}$, had an incubation time of 246 ± 3 days (n/n_0 = 8/8) when inoculated with sCJD(MM1) (RG) prions. Both Tg lines express MHu2M(M165V) at 2–4×.

Tg mouse lines expressing either MHu2M(S96N) or MHu2M(S96N,M165V,E167Q) were not fully established. Instead, individual founders and F1 littermates were inoculated with sCJD(MM1) (RG) prions. Six inoculated Tg(MHu2M,S96N)28386/$Prnp^{0/0}$ mice developed disease at 285 ± 8 days. Two Tg(MHu2M,S96N,M165V,E167Q)34098/$Prnp^{0/0}$ mice inoculated with sCJD(MM1) (RG) prions developed disease after 205 and 364 days.

Four Tg mouse founders and their F1 littermates expressing MHu2M(S96N,M108L,M111V) had incubation times of 160 ± 3 days (n/n_0 = 4/4), 170 ± 5 days (3/3), 229 ± 9 days (3/3), 195 ± 20 days (2/2) when inoculated with sCJD(MM1) (RG) prions. The differences in incubation times between groups may be due to different levels of PrP expression, but in all four experiments, the Tg(MHu2M,S96N,M108L,M111V)34098/$Prnp^{0/0}$ mice showed shorter incubation times than the 285 days noted above for Tg(MHu2M,S96N)28386/$Prnp^{0/0}$ mice.

Transmission of sCJD Prions to Tg(HuPrP) Mice. Tg5378 and Tg(HuPrP,M129)440/$Prnp^{0/0}$ mice with PrP transgenes encoding M at position 129 had shorter incubation times for sCJD(MM1) prions compared with Tg(HuPrP,V129)152/$Prnp^{0/0}$ mice (Table 1). Conversely, only Tg(HuPrP,V129)152/$Prnp^{0/0}$ mice with a transgene encoding V at position 129 could be reproducibly infected with sCJD(VV2) prions (Table 1). Whereas Tg(HuPrP,V129)152/$Prnp^{0/0}$ mice were generally susceptible to human prions with M at

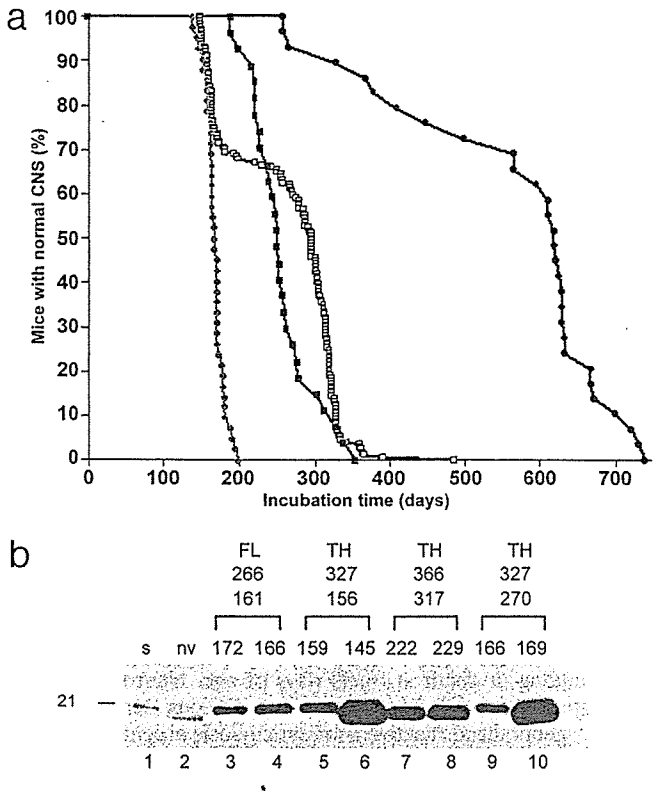

Fig. 3. Serial transmission of vCJD prions into Tg5378 mice. (*a*) Survival curve of Tg5378 mice inoculated with vCJD. The black line with the filled circles represents the first passage into Tg5378 mice, the black line with the open squares depicts the second passage, the blue line shows the third passage of the long-incubating substrain, and the red line illustrates the third passage of the short-incubating substrain. (*b*) Immunoblots of deglycosylated $rPrP^{Sc}$ in selected brains from the third passage of vCJD into Tg5378 mice. The three sets of numbers above the immunoblot represent, from top to bottom, incubation times for first, second, and third passage. For the third passage, deglycosylated $rPrP^{Sc}$ from brains of two different mice are shown. Deglycosylated $rPrP^{Sc}$ from human patients with sCJD(MM1) (lane 1) and vCJD (lane 2) are depicted. Tg mice that were classified as short incubation time on second passage (lanes 3–6, red line in *a*) and as long incubation time on second passage (lanes 7–10, blue line in *a*). Deglycosylated $rPrP^{Sc}$ has the electrophoretic mobility of either 21 kDa (lanes 3–5 and 9) or 19 kDa (lanes 6–8 and 10). The original vCJD prions used to inoculate the mice were either from the frontal lobe (FL) (lanes 3 and 4) or from the thalamus (TH) (lanes 5–10) of the human patient.

position 129, Tg(HuPrP,M129)440/$Prnp^{0/0}$ and Tg5378 mice were marginally susceptible to human prions with V at position 129 (Table 1, compare MM1, MV2, and VV2). Presumably, these results reflect the same mechanism that is responsible for the increased frequency of sCJD in patients that are homozygous for M or V at position 129 (9). For sCJD(MV2) prions, the incubation times were shortest in Tg(HuPrP,V129)152/$Prnp^{0/0}$ mice. Whether this reflects the fact that PrP^{Sc} in these inocula originated from PrP^{C} containing V129 (Table 1) is uncertain. sCJD(MV1) prions transmitted to Tg mice with incubation times similar to those found with sCJD(MM1) prions (Table 1).

Transmission of vCJD Prions to Tg Mice. Tg22372 mice inoculated with brain homogenates of two patients with vCJD exhibited incubation times of 335 ± 23 days and 380 ± 10 days, with the first mouse showing signs of neurologic dysfunction at 254 days after inoculation (Table 1). In contrast, vCJD prions inoculated into Tg5378 mice resulted in prolonged incubation times between 300 and 725 days, with only 25% of the mice becoming ill by 500 days (Fig. 3*a*).

Inocula prepared from different mouse brains, all of which received the same human vCJD inoculum on first passage, produced incubation times ranging between 156 and 308 days on second passage. On second passage of MHu2M(vCJD) prions, the incubation times in Tg5378 mice shortened substantially and showed a biphasic pattern, with mean incubation times of ≈160 days and ≈290 days (Fig. 3*a*), indicating a transmission barrier for at least two different strains of vCJD prions. On third passage, the incubation time of the shorter strain (≈160 days) remained constant, whereas the longer strain (≈290 days) showed a modest shortening of ≈60 days. Of note, all inocula derived from the frontal lobe of one vCJD patient (RU 96/02) resulted in short (≈160 days) incubation times on third passage, whereas inocula from the thalamus of another vCJD patient (RU 96/07) resulted in both long (250–320 days) and short incubation times on third passage. Because only a total of eight second-passage mouse brains inoculated with prions from two vCJD patients were passaged a third time, we are reluctant to assign strain-specific characteristics to particular brain regions. In our initial study of vCJD passaged in Tg5378 mice, we found that on first and second passage, a deglycosylated $rPrP^{Sc}$ fragment of 19 kDa was produced (Fig. 1*a*, lanes 10–12), which has been found in all vCJD cases examined to date. In third-passage mouse brain homogenates, we were surprised to find deglycosylated $rPrP^{Sc}$ fragments of 19 kDa in some brains and of 21 kDa in others (Fig. 3*b*). There was no correlation between the incubation time and the fragment size. In fact, different Tg5378 mice inoculated with the same second-passage mouse brain homogenate had similar incubation times on third passage but different sizes of deglycosylated $rPrP^{Sc}$ fragments (Fig. 3*b*, compare lane 5 with 6, and lane 9 with 10).

Discussion

Mutants of Chimeric PrP with Abbreviated Incubation Times. Unable to shorten the incubation time by increasing the expression of MHu2M, we asked whether changing some residues encoded by the transgene might lead to a shortening of the incubation time. Faced with a very large number of possible mutations that could only be assessed by construction of Tg mice, we focused on the nine residues that distinguish MHu2MPrP from MoPrP. Because MHu2MPrP is converted to PrP^{Sc} in the presence of MoPrP but not HuPrP (4), we decided to revert some of the Hu residues at the N- and C-terminal ends of Hu2 insert (Fig. 5). Changing the two human residues at positions 165 and 167 at the C terminus of the Hu2 insert yielded a transgene product that is responsive to sCJD(MM1) prions, with incubation times between 106 and 124 days. sCJD(MM1) is the most prevalent subclass of sCJD, accounting for ≈68% of cases (20). sCJD(VV2) prions did not transmit as rapidly as sCJD(MM1) prions, presumably reflecting the fact that residue 129 in MHu2M(M165V,E167Q) is M (Table 1). The importance of homology at codon 129 between the recipient and prions in the inoculum also seems to be reflected by the differences in incubation times between Tg(HuPrP,M129)440/$Prnp^{0/0}$ and Tg(HuPrP,V129)152/$Prnp^{0/0}$ mice that received the same inoculum (Table 1).

Mutants of Chimeric PrP with Prolonged Incubation Times. The S96N mutation in MHu2MPrP resulted in a prolongation of the incubation time, which was partially counteracted by introduction of the M108L and M111V mutations (Fig. 5). When the M165V and E167Q mutations were combined with the S96N mutation, the abbreviated incubation times were abolished. This finding suggests that both the N- and C-terminal domains of the Hu2 insert modulate prion replication. Because the M108L and M111V mutations counteracted the prolonged incubation time produced by the S96N mutation, it is reasonable to ask whether either one or both of these mutations might further shorten the abbreviated incubation times observed with M165V and E167Q. It is noteworthy that M108L and M111V mutations have been shown to modulate transmission of prions to Syrian hamsters (33, 34).

Neurodegeneration in Tg Mice Expressing Chimeric PrP. Two Tg lines expressing MHu2MPrP(M165V,E167Q) at ≈4× were constructed. The majority of the offspring from each of these lines developed ataxia between 120 and 150 days of age. Interestingly, the E167Q mutation alone in Tg(MHu2M,E167Q)18990/$Prnp^{0/0}$ mice expressing the transgene product at ≈8× resulted in spontaneous neurodegeneration at ≈300 days of age.

The neurodegeneration observed in Tg mice expressing high levels of either MHu2M(M165V,E167Q) or MHu2M(E167Q) is not unlike some other mutant PrPs expressed at high levels on the $Prnp^{0/0}$ background (35–39). Of note, the neurodegeneration caused by either truncated MoPrP(Δ32–121) or MoPrP(Δ32–134) could be prevented by coexpression of wt MoPrP (40). This is reminiscent of the rescue of mice overexpressing the PrP paralog doppel (Dpl) in the cerebellum; coexpression of either Mo or SHa PrP prevented neurodegeneration (41–43). Whether the coexpression of MoPrP in Tg mice expressing high levels of MHu2M(M165V,E167Q) will prevent neurodegeneration and still enable abbreviated incubation times is unknown. In earlier studies with Tg(MHu2M) mice, the incubation times were similar regardless of whether MoPrP was coexpressed (4, 11).

Species Barriers and Prion Strains. Our results show that homology of the PrP sequence between the host PrP^C and the infecting prion is an imperfect predictor of prion transmission. For example, some sCJD(MM2) prions transmitted inefficiently to Tg(HuPrP,M129)440/$Prnp^{0/0}$ (Table 1) and vCJD prions also transmitted quite inefficiently to Tg5378 mice (Fig. 3). In contrast, vCJD prions readily transmit to Tg(BoPrP)$Prnp^{0/0}$ mice, whereas sCJD prions do not (18). Our findings emphasize the need to consider the tertiary structures of PrP^C and PrP^{Sc} with respect to prion transmission. Although in many cases, homologous PrP^C is able to adopt the conformation of PrP^{Sc}, some strains, such as vCJD, are clear exceptions. The efficient transmission of vCJD prions in Tg(BoPrP)$Prnp^{0/0}$ mice and the rather inefficient transmission to Tg5378 mice (Fig. 3*a*) argue that the conformation of the BSE prion strain was maintained on passage from cattle to humans.

In earlier studies, it was recognized that passage of prions across a species barrier often produced new prion strains (44). Later, the species barrier was shown to be caused by species-specific differences in the PrP sequence of the recipient host and the donor inoculum (10, 30). In the studies reported here, we used the transmission barrier for vCJD prions in Tg5378 mice (Fig. 3*a*) to isolate multiple strains of prions. On second passage in Tg5378 mice, at least two distinct strains of vCJD prions were evident based on the biphasic distribution of incubation times. On third passage, the two vCJD strains were analyzed by determining the molecular size of the $rPrP^{Sc}$ fragment after deglycosylation (Fig. 3*b*). Our findings show no correlation between the size of the PrP^{Sc} fragment and the incubation time, but clearly indicate that several vCJD prion strains can be generated under these circumstances.

Concluding Remarks. Our discovery that Tg22372 mice have incubation times of ≈100 days for sCJD(MM1) prions represents a substantial advance in understanding the molecular basis of the species barrier. In addition, this discovery has practical importance in that end-point titrations of human brain homogenates can be accomplished in <250 days. Such titrations are critical for characterizing human prion strains as well as for calibrating sensitive immunoassays (45).

We thank Cynthia Cowdrey for technical assistance as well as Pierre Lessard and Mike Scott for discussions. This work was supported by grants from the National Institutes of Health as well as by a gift from the G. Harold and Leila Y. Mathers Charitable Foundation. C.K. was supported by a postdoctoral fellowship from the Swiss National Foundation.

1. Prusiner, S. B. (1998) *Proc. Natl. Acad. Sci. USA* **95**, 13363–13383.
2. Prusiner, S. B. (1989) *Annu. Rev. Microbiol.* **43**, 345–374.
3. Kellings, K., Prusiner, S. B. & Riesner, D. (1994) *Philos. Trans. R. Soc. London B* **343**, 425–430.
4. Telling, G. C., Scott, M., Mastrianni, J., Gabizon, R., Torchia, M., Cohen, F. E., DeArmond, S. J. & Prusiner, S. B. (1995) *Cell* **83**, 79–90.
5. Perrier, V., Kaneko, K., Safar, J., Vergara, J., Tremblay, P., DeArmond, S. J., Cohen, F. E., Prusiner, S. B. & Wallace, A. C. (2002) *Proc. Natl. Acad. Sci. USA* **99**, 13079–13084.
6. Kaneko, K., Zulianello, L., Scott, M., Cooper, C. M., Wallace, A. C., James, T. L., Cohen, F. E. & Prusiner, S. B. (1997) *Proc. Natl. Acad. Sci. USA* **94**, 10069–10074.
7. Pattison, I. H. (1965) in *Slow, Latent and Temperate Virus Infections*, National Institute of Neurological Diseases and Blindness Monograph, eds. Gajdusek, D. C., Gibbs, C. J., Jr., & Alpers, M. P. (U. S. Government Printing, Washington, DC), No. 2, pp. 249–257.
8. Scott, M., Foster, D., Mirenda, C., Serban, D., Coufal, F., Wälchli, M., Torchia, M., Groth, D., Carlson, G., DeArmond, S. J., Westaway, D. & Prusiner, S. B. (1989) *Cell* **59**, 847–857.
9. Palmer, M. S., Dryden, A. J., Hughes, J. T. & Collinge, J. (1991) *Nature* **352**, 340–342.
10. Scott, M., Ridley, R. M., Baker, H. F., DeArmond, S. J. & Prusiner, S. B. (1999) in *Prion Biology and Diseases*, ed. Prusiner, S. B. (Cold Spring Harbor Lab. Press, Plainview, NY), pp. 307–347.
11. Telling, G. C., Scott, M., Hsiao, K. K., Foster, D., Yang, S.-L., Torchia, M., Sidle, K. C. L., Collinge, J., DeArmond, S. J. & Prusiner, S. B. (1994) *Proc. Natl. Acad. Sci. USA* **91**, 9936–9940.
12. Asante, E. A., Linehan, J. M., Desbruslais, M., Joiner, S., Gowland, I., Wood, A. L., Welch, J., Hill, A. F., Lloyd, S. E., Wadsworth, J. D. & Collinge, J. (2002) *EMBO J.* **21**, 6358–6366.
13. Bruce, M. E., McBride, P. A. & Farquhar, C. F. (1989) *Neurosci. Lett.* **102**, 1–6.
14. Hecker, R., Taraboulos, A., Scott, M., Pan, K.-M., Torchia, M., Jendroska, K., DeArmond, S. J. & Prusiner, S. B. (1992) *Genes Dev.* **6**, 1213–1228.
15. Bessen, R. A. & Marsh, R. F. (1994) *J. Virol.* **68**, 7859–7868.
16. Telling, G. C., Parchi, P., DeArmond, S. J., Cortelli, P., Montagna, P., Gabizon, R., Mastrianni, J., Lugaresi, E., Gambetti, P. & Prusiner, S. B. (1996) *Science* **274**, 2079–2082.
17. Safar, J., Wille, H., Itri, V., Groth, D., Serban, H., Torchia, M., Cohen, F. E. & Prusiner, S. B. (1998) *Nat. Med.* **4**, 1157–1165.
18. Scott, M. R., Will, R., Ironside, J., Nguyen, H.-O. B., Tremblay, P., DeArmond, S. J. & Prusiner, S. B. (1999) *Proc. Natl. Acad. Sci. USA* **96**, 15137–15142.
19. Peretz, D., Williamson, R. A., Legname, G., Matsunaga, Y., Vergara, J., Burton, D., DeArmond, S. J., Prusiner, S. B. & Scott, M. R. (2002) *Neuron* **34**, 921–932.
20. Parchi, P., Giese, A., Capellari, S., Brown, P., Schulz-Schaeffer, W., Windl, O., Zerr, I., Budka, H., Kopp, N., Piccardo, P., *et al.* (1999) *Ann. Neurol.* **46**, 224–233.
21. Will, R. G., Ironside, J. W., Zeidler, M., Cousens, S. N., Estibeiro, K., Alperovitch, A., Poser, S., Pocchiari, M., Hofman, A. & Smith, P. G. (1996) *Lancet* **347**, 921–925.
22. Collinge, J., Sidle, K. C. L., Meads, J., Ironside, J. & Hill, A. F. (1996) *Nature* **383**, 685–690.
23. Bruce, M. E., Will, R. G., Ironside, J. W., McConnell, I., Drummond, D., Suttie, A., McCardle, L., Chree, A., Hope, J., Birkett, C., *et al.* (1997) *Nature* **389**, 498–501.
24. Scott, M. R., Köhler, R., Foster, D. & Prusiner, S. B. (1992) *Protein Sci.* **1**, 986–997.
25. Büeler, H., Fisher, M., Lang, Y., Bluethmann, H., Lipp, H.-P., DeArmond, S. J., Prusiner, S. B., Aguet, M. & Weissmann, C. (1992) *Nature* **356**, 577–582.
26. DeArmond, S. J., Kretzschmar, H. A. & Prusiner, S. B. (2002) in *Greenfield's Neuropathology*, eds. Graham, D. I. & Lantos, P. L. (Hodder Arnold, London), 7th Ed., pp. 273–323.
27. Carlson, G. A., Ebeling, C., Yang, S.-L., Telling, G., Torchia, M., Groth, D., Westaway, D., DeArmond, S. J. & Prusiner, S. B. (1994) *Proc. Natl. Acad. Sci. USA* **91**, 5690–5694.
28. Muramoto, T., Kitamoto, T., Tateishi, J. & Goto, I. (1992) *Brain Res.* **599**, 309–316.
29. Taraboulos, A., Jendroska, K., Serban, D., Yang, S.-L., DeArmond, S. J. & Prusiner, S. B. (1992) *Proc. Natl. Acad. Sci. USA* **89**, 7620–7624.
30. Prusiner, S. B., Scott, M., Foster, D., Pan, K.-M., Groth, D., Mirenda, C., Torchia, M., Yang, S.-L., Serban, D., Carlson, G. A., *et al.* (1990) *Cell* **63**, 673–686.
31. Mastrianni, J. A., Nixon, R., Layzer, R., Telling, G. C., Han, D., DeArmond, S. J. & Prusiner, S. B. (1999) *N. Engl. J. Med.* **340**, 1630–1638.
32. Dickinson, A. G. & Meikle, V. M. (1969) *Genet. Res.* **13**, 213–225.
33. Priola, S. A., Caughey, B., Race, R. E. & Chesebro, B. (1994) *J. Virol.* **68**, 4873–4878.
34. Supattapone, S., Muramoto, T., Legname, G., Mehlhorn, I., Cohen, F. E., DeArmond, S. J., Prusiner, S. B. & Scott, M. R. (2001) *J. Virol.* **75**, 1408–1413.
35. Telling, G. C., Haga, T., Torchia, M., Tremblay, P., DeArmond, S. J. & Prusiner, S. B. (1996) *Genes Dev.* **10**, 1736–1750.
36. Muramoto, T., DeArmond, S. J., Scott, M., Telling, G. C., Cohen, F. E. & Prusiner, S. B. (1997) *Nat. Med.* **3**, 750–755.
37. DeArmond, S. J., Sánchez, H., Yehiely, F., Qiu, Y., Ninchak-Casey, A., Daggett, V., Camerino, A. P., Cayetano, J., Rogers, M., Groth, D., *et al.* (1997) *Neuron* **19**, 1337–1348.
38. Hegde, R. S., Tremblay, P., Groth, D., Prusiner, S. B. & Lingappa, V. R. (1999) *Nature* **402**, 822–826.
39. Supattapone, S., Bouzamondo, E., Ball, H. L., Wille, H., Nguyen, H.-O. B., Cohen, F. E., DeArmond, S. J., Prusiner, S. B. & Scott, M. (2001) *Mol. Cell. Biol.* **21**, 2608–2616.
40. Shmerling, D., Hegyi, I., Fischer, M., Blattler, T., Brandner, S., Gotz, J., Rulicke, T., Flechsig, E., Cozzio, A., von Mering, C., *et al.* (1998) *Cell* **93**, 203–214.
41. Nishida, N., Tremblay, P., Sugimoto, T., Shigematsu, K., Shirabe, S., Petromilli, C., Erpel, S. P., Nakaoke, R., Atarashi, R., Houtani, T., *et al.* (1999) *Lab. Invest.* **79**, 689–697.
42. Moore, R. C., Mastrangelo, P., Bouzamondo, E., Heinrich, C., Legname, G., Prusiner, S. B., Hood, L., Westaway, D., DeArmond, S. J. & Tremblay, P. (2001) *Proc. Natl. Acad. Sci. USA* **98**, 15288–15293.
43. Rossi, D., Cozzio, A., Flechsig, E., Klein, M. A., Rulicke, T., Aguzzi, A. & Weissmann, C. (2001) *EMBO J.* **20**, 694–702.
44. Kimberlin, R. H., Cole, S. & Walker, C. A. (1987) *J. Gen. Virol.* **68**, 1875–1881.
45. Safar, J. G., Scott, M., Monaghan, J., Deering, C., Didorenko, S., Vergara, J., Ball, H., Legname, G., Leclerc, E., Solforosi, L., *et al.* (2002) *Nat. Biotechnol.* **20**, 1147–1150.

Exp. Anim. 52(4), 339–344, 2003

—Note—

Spontaneous T-cell-rich B-cell Lymphoma in a Cynomolgus Monkey (Macaca fascicularis)

Masaki MICHISHITA[1], Shin-ichiro NAKAMURA[1], Ippei SAKAKIBARA[2], Fumiko ONO[3], Kouji FUJIMOTO[3], Kazusaku KAMIYA[4], Yoshiyuki ISHII[4], Kazuhiko HAYASHI[5], Yasuhiro YOSHIKAWA[4], and Kimimasa TAKAHASHI[1]

[1]Department of Veterinary Pathology, Nippon Veterinary Animal and Science University, 1–7–1 Kyonan-cho, Musashino-shi, Tokyo 180-8602, [2]Tsukuba Primate Center for Medical Science, National Insitute of Infectious diseases, 1 Hachimandai, Tsukuba-shi, Ibaraki 305-0843, [3]The Corporation for Production and Research of Laboratory Primates, 1 Hachimandai, Tsukuba-shi, Ibaraki 305-0843, [4]Department of Biomedical Science, Graduate School of Agricultural and Life Science, University of Tokyo, 1–1–1 Yayoi, Bunkyo-ku, Tokyo 113-8657, and [5]Second Department of Pathology, Okayama University Medical School, 2–5–1 Shikata-cho, Okayama-shi, Okayama 700-8558, Japan

Abstract: *A spontaneous T-cell-rich B-cell lymphoma (TCRBCL) occurred as a subcutaneous mass in the buccal region and enlarged submandibular lymph node in a 6-year-old female cynomolgus monkey (Macaca fascicularis). The constituent cells were examined by histology, immunohistochemistry and the double labeled-immunofluorescence method (dl-IF). Further, in situ hybridization (ISH) was employed to detect the gene expression of Epstein Barr virus (EBV). Histologically, the mass was comprised mainly of neoplastic large lymphoid cells and reactive small mononuclear cells. Immunohistochemically, the neoplastic large lymphoid cells were positive for CD20, CD79α, MHC class II, and either IgG, IgM, or IgA. Polyclonal Ig production by the neoplastic large lymphoid cells was demonstrated by dl-IF, although IgG-positive ones predominanted in number. On the other hand, most of the small mononuclear cells were positive for CD3 and were regarded as reactive T lymphocytes, while the remaining cells appeared to be histocytes or reactive B-cells. Transcripts of EBV gene were not demonstrated in these neoplastic or reactive cells by ISH. This is the first reported case of spontaneous TCRBCL in the cynomolgus monkey.*

Key words: *cynomolgus monkey, spontaneous, T-cell-rich B-cell lymphoma*

Spontaneous lymphomas have infrequently been reported in nonhuman primates, such as chimpanzees, African green monkeys, gibbons, baboons, cynomolgus monkeys, and rhesus monkeys [1, 4, 7, 8, 12, 14–16, 22, 24]. Simian T-cell lymphomas, which are often associated with simian T-cell leukemia virus, have been found in baboons and African green monkey [13, 22], while simian B-cell lymphomas have been reported in

(Received 7 January 2002 / Accepted 26 March 2003)

Address corresponding: K. Takahashi, Department of Veterinary Pathology, Nippon Veterinary Animal and Science University, 1–7–1 Kyonan-cho, Musashino-shi, Tokyo 180-8602, Japan

rhesus monkeys [24]. Although various primate species are latently infected with Epstein Barr virus (EBV) [9] that causes a juvenile type of B-cell lymphoma (Burkitt lymphoma) in humans, there has been no report on spontaneous lymphomas associated with EBV in those species.

T-cell-rich B-cell lymphoma (TCRBCL) has been characterized as a morphological variant of the diffuse B-cell lymphoma group and its criteria is a large B-cell tumor with reactive T-cells occupying more than 50% of the cellular population [19]. Recently, TCRBCL has been reported not only in humans [3, 20, 21] but also in some nonhuman species [2, 6, 17, 23, 26,]. Although it has been reported that EBV was associated with the pathogenesis of TCRBCL in humans [25, 27], such a phenomenon has not been seen in other animal species.

In the present study, spontaneous TCRBCL which occurred in the buccal region of a 3-year and 9-month-old female cynomolgus monkey was studied by histological, immunohistochemical and double-labeled immnofluorescence (dl-IF) examinations. Furthermore, the correlation between TCRBCL and EBV was examined by an *in situ* hybridization (ISH) method.

The mass was first noted in the subcutis of the buccal region of a 3-year and 9-month-old female cynomolgus monkey (*Macaca fascicularis*) being kept for breeding at the Tsukuba Primate Center for Medical Science, National Institute of Infectious Diseases, Japan. X-ray examination showed an osteolytic pattern of the maxillary bone surrounding the mass. Thereafter, in addition to the mass, an enlarged submandibular lymph node was found and surgically removed when the animal was 5 years and 9 months old. However, the complete removal of the buccal mass was difficult because it was tightly attached to the adjacent tissue. The monkey had clinically poor appetite and diarrhea. Hematology and blood biochemistry revealed leukocytosis and high levels of lactate dehydrogenase. Serologically, a positive antibody reaction against EBV was shown. After surgical removal, the tumors recurred in the same portions. The animal was euthanatized because of poor prognosis when she was 6 years old.

At necropsy, the primary buccal mass and enlarged mandibular lymph node were about 7 cm in diameter, respectively. The cut surfaces were homogeneously grayish white. No metastasis of the tumor to other organs was confirmed macroscopically.

Tissue samples were fixed in 20% neutral buffered formalin, embedded in paraffin, and sectioned 3 μm in thickness. Deparaffinized sections were stained with hematoxylin and eosin (HE), and further subjected to other stains as necessary.

Some deparaffinized sections were used for immunohistochemistry. Primary antibodies used in the present study were monoclonal antibodies against human CD20, CD79α, MHC class II (HLA-DR), HAM56, MAC387 and swine vimentin, and polyclonal antisera against human CD3, IgG, IgA, IgM, lysozyme and C3c complement (Table 1). Antisera against human CD3, IgG, and lysozyme are known to be also applicable to primates [12]. For detecting some antigens, sections were pretreated with 1% trypsin and with subsequent hydrated autoclave or microwave methods. Secondary antibodies used were biotinylated goat antisera (DAKO, Denmark) against mouse or rabbit immunoglobulin (Ig). These sections were reacted with peroxidase-conjugated streptavidin (LSAB, DAKO) and visualized with 3.3'-diaminobenzidine tetrahydrochloride (Dojindo, Japan) plus hydrogen peroxidase. The mean value (%) of CD3-positive small mononuclear cells per whole cellular population was determined by counting microscopically in at least 7 different fields of 400X magnification.

For the double-labeled immunofluorescence method, a combination of an indirect method with mouse monoclonal antibody to human IgG (DAKO, Denmark) and Texas red-conjugated goat antiserum to mouse IgG (Vecter, USA) and a direct method with FITC-conjugated polyclonal antisera against human IgA or IgM (DAKO, Denmark) was employed. Stained sections were observed under a confocal laser microscope (Laser Scanning Microscope 510, Carl Zeiss, Germany).

To detect EBV-encoded small RNA-1 (EBER-1), ISH was employed using single-stranded FITC-labeled 30-base oligonucleotide probes, complementary (antisense probe, 5'-AGACACCGTCCTCACCACCCGGGACT TGTA-3') or anticomplementary (sense, negative control probe) [5]. Formalin-fixed, paraffin-embedded sections from the buccal mass and mandibular lymph node were hybridized with the sense or antisense probe. They were further visualized using a commercialized *in situ* hybridization kit (DAKO, Denmark), as described previously [11].

The tumor was composed of two types of cells,

Table 1. Antibodies used in the present study

Antibody	Source	Dilution
Mouse monoclonal antibodies against		
Human B Cell, CD20, BLA36	BioGenex	1:1000
Human B Cell, CD79α, HM57	DAKO	1:25
Human HLA-DR, Alpha-Chain	DAKO	1:50
Human Macrophage, HAM 56	DAKO	1:50
Human Myeloid/Histiocyte Antigen, MAC387	DAKO	1:100
Swine Vimentin, V9	DAKO	1:50
Human IgG	ZYMED	1:500
Rabbit polyclonal antisera against		
Human T Cell, CD3	DAKO	1:300
Human IgG (Gamma-Chains)	DAKO	1:500
Human IgA (Alpha-Chains)	DAKO	1:300
Human IgM (Mu-Chains)	DAKO	1:300
Human lysozyme	DAKO	1:300
Human C3c Complement	DAKO	1:100

Table 2. Immunohistochemical characteristics of the present lymphoma

	CD20	CD79α	IgG	IgA	IgM	HLA-DR	CD3	HAM56	MAC387	lysozyme	vimentin
Neoplastic large cell	+	±	+	+	+	+	−	−	−	−	+
Small cell	±	±	−	−	±	±	+	+	+	+	+

+, positive; ±, partly positive; −, negative

namely neoplastic large lymphoid cells and well-differentiated small mononuclear cells, both of which were distributed diffusely (Fig. 1). The neoplastic large lymphoid cells were relatively pleomorphic in shape, and had slightly eosiophilic, abundant cytoplasm with frequent vacuoles. They had a large, hypochromatic nucleus with plural large nucleoli. Some of these cells contained PAS-positive substances in the perinuclear area. Neoplastic multinucleated giant cells were occasionally observed (Fig. 2). On the other hand, the small mononuclear cells showed oval or elongated shape, and had scant cytoplasm. Their nuclei were round or oval, and uniformly hyperchromatic. Neither nuclear atypia nor mitotic figure was observed in the small mononuclear cells. The submandibular lymph node also showed histological changes similar to the buccal mass. The original structure of the lymph node was almost destroyed by proliferation of these tumor cells. Histopathological findings of the mass excised surgically while alive were similar to those of the tumor obtained at necropsy.

Both neoplastic large lymphoid cells and multinucleated giant cells were positive for CD20 (Fig. 3), CD79α, IgG (Fig. 4), IgA, IgM, and vimentin (date not shown), but negative for CD3. Thus, these cells exhibited the character of B lymphocyte with various Ig production. Furthermore they were slightly positive for HLA-DR (Fig. 5). A large number of the small mononuclear cells were, in contrast, positive for CD3 (Fig. 6), whereas a small population of them was also positive for CD20, CD79α, HLA-DR, IgM, HAM56, lysozyme (Fig. 7) and/or MAC387 (Table 2). Especially, CD3-positive small cells occupied 53% of the whole cellular population. Therefore, these small mononuclear cells were considered to be predominantly T-cells, with a very small number of histiocytic cells and non-neoplastic B-cells.

By dl-IF, it was revealed that the neoplastic large lymphoid cells were predominantly IgG-positive, but occasionally IgA- or IgM- positive. In addition, a few of the large lymphoid cells were double-labeled, in a combination of IgG+IgA or IgG+IgM (Fig. 8).

EBER-1 transcripts could not be detected in any neoplastic large lymphoid or reactive small mononuclear